SLAC-PUB-1634
August 1975
(E)

EXTRACTION OF THE STRUCTURE FUNCTIONS AND $R = \sigma_L/\sigma_T$ FROM DEEP INELASTIC e-p AND e-d CROSS SECTIONS*

E. M. Riordan, A. Bodek†, M. Breidenbach‡, D. L. Dubin, J. E. Elias§, J. I. Friedman, H. W. Kendall, J. S. Poucher††, and M. R. Sogard‡‡

Department of Physics and Laboratory for Nuclear Science
Massachusetts Institute of Technology, Cambridge, Massachusetts 02139

and

D. H. Coward and D. J. Sherden

Stanford Linear Accelerator Center
Stanford University, Stanford, California 94305

ABSTRACT

The two structure functions W_1 and W_2 and $R = \sigma_L/\sigma_T$ are extracted from deep inelastic e-p and e-d cross sections measured in three experiments at the Stanford Linear Accelerator Center. The data for these quantities cover the kinematic range $2M < W < 4.84$ GeV, $2.1 < \nu < 13.4$ GeV, $1.0 \leq Q^2 \leq 16.0$ GeV^2, and $0.1 \leq x \leq 0.8$, where $x = Q^2/2M\nu = 1/\omega$ and M is the proton mass. The quantities R_p and R_d are found to be equal, within the statistical errors and systematic uncertainties of these measurements. The kinematic behavior of R_p is examined in detail. For $x \geq 0.25$, the behavior of νR_p is consistent with scaling, indicative of spin-1/2 constituents, in a parton model of the proton. Evidence is found for deviations from scaling in both ω and $\omega' = 1 + W^2/Q^2$ of both proton structure functions $2MW_1^p$ and νW_2^p.

(Contributed paper to the International Symposium on Lepton and Photon Interactions, Stanford, California, 21 - 27 August 1975)

---

* Work supported by the U. S. Energy Research and Development Administration under Contract Nos. E(11-1)-3069 and E(04-3)-515.

Present address:
† Department of Physics, California Institute of Technology, Pasadena, California 91109.
‡ Stanford Linear Accelerator Center, Stanford, California 94305.
§ National Accelerator Laboratory, Batavia, Illinois 60510.
†† Department of Physics and Astronomy, Vanderbilt University, Nashville, Tennessee 37235.
‡‡ Laboratory of Nuclear Studies, Cornell University, Ithaca, New York 14850.

I. INTRODUCTION

We have measured the differential cross sections for inelastic electron-proton (e-p) and electron-deuteron (e-d) scattering using the 8 GeV spectrometer at the Stanford Linear Accelerator Center (SLAC). The cross sections were measured in two separate experiments at laboratory scattering angles of 15, 18, 19, 26, and 34 degrees. Partial results of these experiments, particularly the ratio of neutron to proton cross sections, σ_n/σ_p, have already been reported.[1,2,3,4] Inelastic e-p and e-d cross sections measured earlier[5,6] with the SLAC 20 GeV spectrometer were included in the present analysis. The cross sections from all three experiments permit an accurate separation of the two structure functions W_1 and W_2 and the quantity $R = \sigma_L/\sigma_T$ over a larger kinematic range than was previously accessible.[3,4,7]

In these experiments, an electron of incident energy E scatters from a nuclear target through a laboratory angle θ to a final energy E', and only the electron is detected in the final state. In the first Born approximation, the scattering occurs through the exchange of a single virtual photon of energy $\nu = E - E'$ and invariant momentum transfer $q^2 = -4EE' \sin^2\theta/2 = -Q^2$ as in Figure 1. The hadronic final state is unknown except for its invariant mass $W = (M^2 + 2M\nu - Q^2)^{\frac{1}{2}}$, where M is the proton mass. The differential cross section for electron scattering from a nuclear target is related to the two structure functions W_1 and W_2 according to[8]

$$\frac{d^2\sigma}{d\Omega dE'}(E, E', \theta) = \sigma_M \left\{ W_2(\nu, Q^2) + 2W_1(\nu, Q^2) \tan^2\theta/2 \right\} \qquad \text{(I. 1)}$$

where

$$\sigma_M = \frac{4\alpha^2 (E')^2}{Q^4} \cos^2\theta/2 \quad \text{is the Mott cross section.}$$

The structure functions W_1 and W_2 are similarly defined by Eq. (I. 1) for proton, deuteron, and neutron targets; they summarize all the information obtainable about the structure of these particles from unpolarized electron scattering.

Within the single-photon exchange approximation, one may alternatively view inelastic electron scattering as virtual photoproduction. Here, as opposed to real photoproduction, the photon mass q^2 is variable and the exchanged photon may have a longitudinal as well as a transverse polarization. If the final state hadrons are not observed, the differential cross section for inelastic electron scattering is related to the total cross sections for absorption of transverse and longitudinal virtual photons according to[9]

$$\frac{d^2\sigma}{d\Omega dE'}(E, E', \theta) = \Gamma \left\{ \sigma_T(\nu, Q^2) + \epsilon \sigma_L(\nu, Q^2) \right\} \tag{I. 2}$$

where

$$\Gamma = \frac{\alpha}{4\pi^2} \left(\frac{K}{Q^2} \right) \left(\frac{E'}{E} \right) \left(\frac{2}{1-\epsilon} \right) ,$$

$$\epsilon = \left\{ 1 + 2(1+\nu^2/Q^2)\tan^2\theta/2 \right\}^{-1}, \quad \text{and} \quad K = \frac{W^2 - M^2}{2M} .$$

The quantity Γ is the flux of transverse virtual photons and ϵ is the polarization parameter. The cross sections σ_T and σ_L are related to the structure functions W_1 and W_2 by

$$\begin{aligned} W_1(\nu, Q^2) &= \frac{K}{4\pi^2\alpha} \sigma_T(\nu, Q^2) \\ W_2(\nu, Q^2) &= \frac{K}{4\pi^2\alpha} \left(\frac{Q^2}{Q^2+\nu^2} \right) \left\{ \sigma_T(\nu, Q^2) + \sigma_L(\nu, Q^2) \right\} \end{aligned} \tag{I. 3}$$

In the limit as $Q^2 \to 0$, $\sigma_L \to 0$ and $\sigma_T \to \sigma_\gamma(\nu)$, the real photoproduction cross section. The quantity R, defined as the ratio σ_L/σ_T, is related to the structure functions by

$$R \equiv \frac{\sigma_L}{\sigma_T} = \frac{W_2}{W_1}(1 + \nu^2/Q^2) - 1 \tag{I.4}$$

Eqs. (I.1) through (I.4) apply equally well for proton, deuteron, or neutron targets. Extraction of W_1 and W_2 at some (ν, Q^2), which is equivalent to the extraction of W_2 and $R = \sigma_L/\sigma_T$, requires differential cross sections for at least two values of the scattering angle θ.

The emphasis in this paper is placed upon the behavior of R, W_1, and W_2 in the Bjorken limit $\nu \to \infty$, $Q^2 \to \infty$, with $\omega = 1/x = 2M\nu/Q^2$ held fixed. Studies of the behavior of these quantities using portions of the present data have already been reported.[3,4] The results presented here represent a much more complete study of these quantities; they are consistent with the earlier results.

II. THE EXPERIMENTS

Cross sections for inelastic e-p and e-d scattering were measured over a range of scattering angles in two separate experiments that employed similar experimental apparatus and data analysis methods. Electrons of fixed primary energy scattered from liquid hydrogen and deuterium targets and were momentum-analyzed in a focusing spectrometer set at fixed scattering angles. A number of spectra, each covering a range of E' for fixed values of E, were measured at each angle to permit model-independent radiative corrections to be made. In experiment A[1,3,4] cross sections were measured with the SLAC 8 GeV spectrometer at scattering angles of 18, 26, and 34 degrees. Incident energies ranged from 4.5 GeV to 18.0 GeV and scattered energies ranged from 1.0 to 8.75 GeV, as shown in Fig. 2. Earlier inelastic e-p cross section measurements[7] were repeated with improved statistical accuracies (frequently ±2% errors); inelastic e-d cross sections were measured simultaneously at the same kinematics. The momentum transfer Q^2 ranged from 0.5 GeV^2 to 20.0 GeV^2 and W ranged as high as 5.2 GeV in this experiment. In experiment B,[2] inelastic e-p and e-d cross sections were measured with the 8 GeV spectrometer at scattering angles of 15, 19, 26, and 34 degrees. Incident energies ranged from 8.7 GeV to 20.0 GeV; the ranges of E' measured at each energy and angle are shown in Fig. 3. The momentum transfer Q^2 ranged from 4.0 GeV^2 to 21.8 GeV^2 while W ranged up to 4.1 GeV. This experiment improved the accuracy of the e-p and e-d cross section measurements for $\omega \lesssim 2$ at 26 and 34 degrees and provided completely new data at 15 and 19 degrees.

The experimental setup used to measure inelastic e-p and e-d scattering is shown in Fig. 4. An essentially monochromatic beam of multi-GeV electrons from the Stanford Linear Accelerator was momentum-analyzed and collimated

in the beam switchyard and passed through liquid hydrogen and deuterium target cells on the pivot in End Station A. The SLAC 1.6 GeV spectrometer, set to detect elastic and quasi-elastic recoil protons, was used to monitor the target densities. Two precision toroidal charge monitors were used to measure the flux of incident electrons; they were periodically calibrated against a Faraday cup which was normally out of the beam line. Momentum analysis of scattered particles was accomplished with the SLAC 8 GeV spectrometer set to the desired angle. The spectrometer focused scattered particles upon hodoscopes and trigger counters located in a shielded cave just behind the spectrometer magnets. Also inside the cave, a threshold gas Cerenkov detector and a π-e discriminator separated electrons from a background consisting mostly of pions. The π-e discriminator consisted of totally absorbing lead-lucite shower counter and two counters that sampled the early shower development. Signals from the various devices were assembled in the counting house under the control of an SDS 9300 computer, which logged events from fast electronic logic onto magnetic tape for later analysis. More detailed information on the SLAC 8 GeV spectrometer facility and the beam and charge monitors may be found in the references describing earlier experiments[7,10] which used this spectrometer, and in the Ph.D. theses of A. Bodek[11] and E. M. Riordan.[12]

In both experiments, the measured cross sections were derived from the number of electrons scattered into the spectrometer acceptance for each setting of E, E', and θ. Cell-wall contributions to the cross sections were determined using empty replica targets and were subtracted. Measurements with hydrogen, deuterium, and replica targets were interleaved to minimize systematic differences. The contributions from background processes such as π_0-decay and pair-production were determined by reversing the spectrometer

polarity and measuring the yield of positrons. Radiative corrections were then applied in two steps to extract the cross sections for inelastic e-p and e-d scattering at the selected (E, E', θ). In the first step, the radiative tails from elastic e-p and from elastic and quasi-elastic e-d scattering were subtracted from the measured e-p and e-d cross sections. Inelastic radiative tails were then calculated using a model-independent method and subtracted.

In order to extend the separation of R and the structure functions to $\omega > 5$, inelastic e-p and e-d cross sections measured in an earlier SLAC experiment[5,6] (referred to as experiment C) at scattering angles of 6 and 10 degrees were used in the present analysis. Separation of the structure functions and $R = \sigma_L/\sigma_T$ was then possible over the kinematic region $0.1 \leq x \leq 0.8$ with $1 \leq Q^2 \leq 16$ GeV^2 and $1.8 \leq W \leq 5$ GeV. These separations required a careful normalization of these experiments, as all three experiments used different target cells, and experiment C used the SLAC 20 GeV spectrometer. Experiment B was normalized to experiment A by comparing inelastic cross sections measured at similar kinematics. Experiment C was normalized to experiment A by comparing elastic e-p cross sections measured in the two experiments.[12]

Examples of νW_2^p and νW_2^d, which were calculated from the radiatively corrected e-p and e-d differential cross sections of experiment B by assuming[3,7] $R_p = R_d = 0.18$, are plotted versus W in Figures 5 and 6. The statistical accuracy and kinematic range of these most recent measurements are evident in these plots. The error bars shown in the figures represent only the random errors from counting statistics. The solid lines through the data points are universal fits to the data that will be discussed in a forthcoming publication.[13] The separation of R and the structure functions in the deep inelastic region did not require such a fine resolution as is evident in these figures. Consequently,

the cross-section data for $W \geq 1.8$ GeV were combined into statistically more accurate cross sections by averaging groups of neighboring cross sections at each incident energy at 15°, 19°, and 26°. In experiment A, only a few cross sections for $1.8 \leq W \leq 2.0$ GeV at 18° were averaged in this manner.

Besides the random errors from counting statistics, the random fluctuations in the properties of the beam, the target apparatus, the spectrometer, and the various monitors contributed to the random errors in the cross sections. These contributions were included in the random error in the averaged cross sections, because they contributed to the random error in the separated R and the structure functions. They included random fluctuations in target density (± 0.3%), charge monitors (± 0.3%), incident beam energy (± 0.1% to ± 0.8%) and direction (± 0.1% to ± 1.1%), spectrometer magnet currents (0 to ± 0.5%), and detector efficiencies (± 0.5% to ± 1.0%). The random error from counting statistics normally dominated the error from such random fluctuations, which was typically 1% when all contributions were added in quadrature.

Systematic uncertainties in the cross sections fell into two categories: overall normalization uncertainties and relative uncertainties - those which had a possible kinematic variation. The overall normalization uncertainties did not affect the kinematic variation of R and the structure functions, except through an overall normalization difference between the two experiments. They included the uncertainties in the spectrometer acceptance[12] (± 1.5%), in the target density normalization (± 0.7% and ± 0.9% for hydrogen and deuterium targets in experiment A; ± 0.4% and ± 0.7% in experiment B), in the target length (± 0.6% in experiment A and ± 0.4% in experiment B), and the overall normalization uncertainty (± 3%) in the radiative corrections.[13] Added in quadrature, these uncertainties gave an overall normalization uncertainty of 3.4% to 3.6% in the

inelastic e-p and e-d cross sections from the two experiments. Relative uncertainties in these cross sections included uncertainties in the absolute calibration of the incident energy (± 0.1% to ± 0.8%), in the calibration of E' versus E (± 0.1% to ± 1.0%), in the electron detection efficiency (± 0.5% to ± 1.0%), in the cross-section averaging procedure (0 to ± 1.0%), in the E' dependence of the spectrometer acceptance (0 to ± 1.0%), and the relative uncertainty (± 1% to ± 5%) in the radiative corrections.[13] Added in quadrature, they amounted to a relative uncertainty of not more than 5.5% in the inelastic e-p and e-d cross sections.

Before the cross sections from experiments B and C were used together with those from experiment A to extract R and the structure functions, they were multiplied by normalization factors to account for overall normalization differences among the three experiments. The normalization factors N^p_{AB} and N^d_{AB} of experiment B to experiment A were estimated by comparing cross sections that had been measured at similar E and E' at scattering angles of 26 and 34 degrees in both experiments. Ratios of e-p and e-d cross sections at each common kinematic point were taken to define the normalization factors; the two were always within one standard deviation of their average value at that point. Averaged over the entire set of common kinematic points, the normalization factors were $N^p_{AB} = 1.010 \pm 0.010$ and $N^d_{AB} = 1.010 \pm 0.007$, where the quoted errors are purely random errors. No clear-cut evidence could be found[13] for any kinematic variation of N^p_{AB} and N^d_{AB}. The normalization factor N^p_{AC} was estimated by comparing[12] elastic e-p cross sections that had been measured in experiments A and C.[14] A fit to the elastic e-p cross sections measured in experiment A was on the average 1.9% higher than the elastic e-p cross sections measured in experiment C. Systematic uncertainties of 1.4% in N^p_{AC} arose

from effects that could alter the elastic and inelastic cross sections differently.[12,13] These uncertainties were added in quadrature to the random error, resulting in a value $N^p_{AC} = 1.019 \pm 0.017$. A determination of the normalization factor N^d_{AC} from quasi-elastic e-d cross sections was judged infeasible due to uncertainties arising both from inelastic background subtractions and from corrections for deuteron binding effects. The proton normalization factor was consequently applied to the deuteron cross sections of experiment C, $N^d_{AC} = 1.019 \pm 0.024$, with an additional systematic uncertainty of ± 0.016 already added in quadrature to account for additional uncertainties in the target lengths and densities.

III. SEPARATION OF R AND THE STRUCTURE FUNCTIONS

Separation of W_1 and W_2 (or equivalently σ_L and σ_T) at fixed (ν, Q^2) requires differential cross sections $\frac{d^2\sigma}{d\Omega dE'}(\nu, Q^2, \theta)$ for at least two values of the scattering angle. According to Eq. (I.2), σ_L is the slope and σ_T the $\epsilon = 0$ intercept of a linear fit to

$$\Sigma(\nu, Q^2, \theta) = \frac{1}{\Gamma}\frac{d^2\sigma}{d\Omega dE'} = \sigma_T(\nu, Q^2) + \epsilon(\nu, Q^2, \theta)\sigma_L(\nu, Q^2). \qquad \text{(III.1)}$$

The structure functions and R are readily calculated from σ_L and σ_T according to Eqs. (I.3) and (I.4). There were, however, only a few kinematic points (ν, Q^2) at which the differential cross sections had been directly measured for two or more values of θ. Consequently, values of Σ and its error were obtained by interpolation of the cross sections measured at each angle to selected kinematic points (ν, Q^2) that fell within the overlaps of two or more of the data triangles measured in the three experiments. The kinematic region of $Q^2 - W^2$ space spanned by these overlaps of the measured data triangles is shown in Fig. 7. An array of 75 kinematic points (ν, Q^2), chosen to reflect the distribution of measured cross sections, was used in a systematic study of R and the structure functions. As shown in Fig. 7, these points lie at the intersections of contours of constant - x $(0.1 \leq x \leq 0.8)$ and constant - Q^2 $(1.0 \leq Q^2 \leq 16.0\ \text{GeV}^2)$ with $W > 2M$. A subset of the above $x - Q^2$ array, containing 51 (ν, Q^2) points with $0.2 \leq x \leq 0.8$ and $2.0 \leq Q^2 \leq 16.0\ \text{GeV}^2$, was used in a parallel study wherein only cross sections from experiments A and B were used to extract R and the structure functions. Only the results from the full $x - Q^2$ array are reported in any detail. The results obtained for the restricted $x - Q^2$ array were in general consistent with those of the full $x - Q^2$ array reported here. Previous separations of R and the structure functions using cross sections from

experiments A and C have been reported earlier[3,4,12] and are consistent with the present results, which supersede the earlier ones.

The e-p and e-d cross sections from experiments A and B were used to permit interpolations at five different values of the scattering angle. Where they existed for $\omega \lesssim 2$ at 26° and 34°, the cross sections from experiment B were used in lieu of those from experiment A. Prior to the interpolations, all cross sections from experiment B were multiplied by the normalization factor $N_{AB} = 1.010$. In this way, triangles of cross section data were assembled at $\theta = 15^{\circ}$, 18°, 19°, 26°, and 34°. In order to extend the accessible kinematic region to $x < 0.2$ and to extend the ranges of Q^2 and ϵ available for $x \geq 0.2$, cross sections measured at 6° and 10° in experiment C[5,6] were also used in this analysis. These cross sections had been radiatively corrected by the same method as had been used for experiments A and B; they were then multiplied by $N_{AC} = 1.019$ to normalize them to those of experiment A.

Values of $\Sigma(\nu, Q^2, \theta)$ and its random error were obtained by an interpolation scheme that made no a priori assumptions about the behavior of R. Because this scheme effectively averages 16 cross section measurements for each (ν, Q^2, θ), the values of $\Sigma(\nu, Q^2, \theta)$ and its errors are correlated for neighboring kinematic points (ν, Q^2). In practice, these correlations are difficult to remove, and the distribution of kinematic points (ν, Q^2) was chosen to minimize them. As many as five values of $\Sigma(\nu, Q^2, \theta)$ for five values of $\epsilon(\nu, Q^2, \theta)$ were available at a given kinematic point (ν, Q^2). In general, the accuracy of the separated quantities varied inversely as the range $\Delta\epsilon$ of the variable ϵ spanned by the cross sections for fixed (ν, Q^2). In these separations, $\Delta\epsilon$ ranged from 0.16 to 0.57, while ϵ itself ranged from 0.24 to 0.98.

A. Separation of R_p and R_d

The quantities σ_L and σ_T were available as the parameters of a linear least-squares fit to $\Sigma(\nu, Q^2, \theta)$ versus (ν, Q^2, θ) at each kinematic point (ν, Q^2). In general, the confidence level for these fits was quite good; in only a few instances did χ^2 deviate from the number of degrees of freedom n_D of the fit by more than $(2n_D)^{\frac{1}{2}}$. The quantity $R = \sigma_L/\sigma_T$ is presented for the proton in Table 1, along with estimates of the systematic uncertainty ΔR_p. Five separate contributions to the systematic uncertainty in R_p are also listed in Table 1. The uncertainty ΔR_p^1 arising from the uncertainty of 0.010 in N_{AB}^p was estimated by repeating the extractions using instead a normalization factor $N_{AB}^p = 1.020$. A similar procedure was used to estimate the uncertainty ΔR_p^2 arising from the uncertainty of 0.017 in N_{AC}^p. The uncertainty ΔR_p^3 arising from a possible E' dependence of the spectrometer acceptance was estimated[12] using a redefined acceptance that varied by at most 1% from its nominal value. The uncertainty ΔR_p^4 due to relative uncertainties in detector efficiencies was estimated using redefined efficiencies that varied from their nominal value by at most 1%. The radiative correction uncertainty ΔR_p^5 was estimated by adjusting all proton cross sections by an amount $\Delta\sigma$ determined for each incident energy and angle according to $\Delta\sigma/\sigma = 0.015(E'_{el}(E, \theta)/E')$, where E'_{el} is the energy of elastically scattered electrons,[13] and repeating the extraction of R_p. These five contributions were added in quadrature to obtain the total uncertainty ΔR_p reported in Table 1. The present values of R_p are consistent with those reported earlier;[3,12] much more accurate data are presented for $\omega \lesssim 2$ than were available before.

Values of R_d are also listed in Table 1; they were extracted from the interpolated deuteron cross sections using the same procedure as used for the

proton. The five contributions to the systematic uncertainty in R_d were calculated in the same manner as for R_p, except that uncertainties of 0.007 and 0.024 in the deuteron normalization factors N^d_{AB} and N^d_{AC} were used. They were added in quadrature to obtain the total uncertainty ΔR_d listed.

The weighted averages of R_p and R_d over the full $x - Q^2$ array provide a rough comparison of these quantities. We find $\bar{R}_p = 0.138 \pm 0.011$, with a total systematic uncertainty $\Delta\bar{R}_p = 0.056$, and $\bar{R}_d = 0.175 \pm 0.009$, with a total systematic uncertainty $\Delta\bar{R}_d = 0.060$. Within the normalization uncertainty of experiment C alone, $\bar{R}_d$ is consistent with being equal to $\bar{R}_p$. When the weighted averages are taken only over the restricted $x - Q^2$ array, using only data from experiments A and B, we find $\bar{R}_p = 0.136 \pm 0.017$ and $\bar{R}_d = 0.137 \pm 0.013$.

A more detailed and accurate comparison of R_p, R_d, and R_n was achieved by extracting the quantity $\delta = R_d - R_p$ from the ratio of differential cross sections σ_d/σ_p in a method[12] that exploited the small systematic uncertainty in this ratio. From Eq. (I.2) we get

$$\frac{\sigma_d}{\sigma_p} = T(1 + \epsilon'\delta) \tag{III.2}$$

where $T = \sigma_{Td}/\sigma_{Tp}$ and $\epsilon' = \epsilon/(1 + \epsilon R_p)$. The physical meaning of Eq. (III.2) is clear: a difference between R_d and R_p results in a slope in σ_d/σ_p plotted versus ϵ' (or, essentially, versus ϵ). The connection between R_n and δ is achieved through an expression[11] that exploits the observation that the smearing correction is empirically the same for W_1 and W_2

$$R_n = R_d + \frac{\delta}{Z} \tag{III.3}$$

where $Z = W^n_{1s}/W^p_{1s}$ is the ratio of smeared W^n_1 to smeared W^p_1. In practice, Eq. (III.3) is not very useful if $\delta \neq 0$, for Z is also an unknown. But if $\delta = 0$,

TABLE 1

Extracted values of R_p, R_d, and δ with random errors and estimated systematic uncertainties.

x	Q^2	W	R_p	ΔR_p	ΔR_p^1	ΔR_p^2	ΔR_p^3	ΔR_p^4	ΔR_p^5	R_d	ΔR_d	δ	$\Delta\delta$
0.10	1.00	3.14	0.175±0.132	0.081	0.0	0.036	0.026	0.023	0.063	0.120±0.093	0.082	-0.022±0.171	0.032
0.10	1.25	3.48	0.338±0.155	0.092	0.0	0.036	0.025	0.022	0.078	0.181±0.118	0.074	-0.135±0.200	0.030
0.10	1.50	3.79	0.302±0.127	0.092	0.0	0.034	0.025	0.020	0.079	0.289±0.112	0.087	-0.012±0.184	0.028
0.10	2.00	4.35	0.442±0.199	0.103	0.0	0.028	0.019	0.018	0.096	0.273±0.130	0.090	-0.123±0.232	0.034
0.10	2.50	4.84	0.880±0.844	0.229	0.0	0.115	0.074	0.070	0.171	0.297±0.449	0.182	-0.456±0.881	0.220
0.15	1.00	2.56	0.408±0.159	0.138	0.0	0.094	0.054	0.055	0.064	0.479±0.161	0.167	0.033±0.237	0.090
0.15	1.25	2.82	0.205±0.108	0.102	0.0	0.069	0.038	0.040	0.051	0.377±0.102	0.148	0.201±0.179	0.088
0.15	1.50	3.06	0.095±0.089	0.077	0.0	0.049	0.027	0.028	0.045	0.359±0.118	0.115	0.276±0.203	0.070
0.15	2.00	3.49	0.321±0.096	0.099	0.0	0.061	0.032	0.034	0.063	0.518±0.129	0.131	0.123±0.185	0.065
0.15	2.50	3.88	0.383±0.175	0.130	0.0	0.088	0.042	0.049	0.070	0.471±0.148	0.167	0.078±0.231	0.091
0.15	3.00	4.23	0.332±0.217	0.124	0.0	0.082	0.038	0.045	0.071	0.252±0.142	0.137	-0.060±0.245	0.075
0.15	3.50	4.55	0.174±0.230	0.110	0.0	0.071	0.032	0.033	0.066	0.317±0.173	0.145	0.149±0.303	0.083
0.20	1.00	2.21	0.146±0.107	0.128	0.0	0.097	0.048	0.055	0.039	0.180±0.093	0.168	0.028±0.146	0.098
0.20	1.25	2.42	0.246±0.118	0.136	0.0	0.104	0.048	0.057	0.045	0.267±0.105	0.171	-0.084±0.147	0.086
0.20	1.50	2.62	0.457±0.140	0.151	0.0	0.115	0.049	0.062	0.058	0.483±0.119	0.191	0.009±0.189	0.109
0.20	2.00	2.98	0.218±0.075	0.085	0.0	0.057	0.031	0.033	0.045	0.336±0.073	0.106	0.074±0.113	0.053
0.20	2.50	3.30	0.071±0.072	0.075	0.0	0.054	0.021	0.028	0.037	0.250±0.090	0.109	0.148±0.143	0.062
0.20	3.00	3.59	0.171±0.111	0.098	0.0	0.073	0.028	0.038	0.043	0.277±0.096	0.134	0.102±0.158	0.079
0.20	3.50	3.86	0.261±0.158	0.109	0.0	0.083	0.027	0.042	0.048	0.465±0.151	0.164	0.202±0.244	0.103
0.20	4.00	4.11	0.127±0.122	0.093	0.0	0.071	0.022	0.035	0.043	0.439±0.129	0.154	0.325±0.209	0.102
0.25	1.00	1.97	0.439±0.186	0.255	0.0	0.206	0.086	0.109	0.055	0.426±0.152	0.325	-0.001±0.243	0.194
0.25	1.25	2.15	0.106±0.113	0.135	0.0	0.109	0.044	0.058	0.033	0.184±0.101	0.197	0.063±0.160	0.116
0.25	1.50	2.32	0.307±0.125	0.155	0.0	0.125	0.047	0.065	0.045	0.378±0.109	0.219	0.048±0.170	0.129
0.25	2.00	2.62	0.233±0.083	0.096	0.0	0.072	0.033	0.039	0.038	0.346±0.082	0.129	0.140±0.134	0.078
0.25	2.50	2.89	0.196±0.117	0.103	0.0	0.083	0.025	0.041	0.037	0.316±0.135	0.146	-0.041±0.176	0.070
0.25	3.00	3.14	0.179±0.090	0.089	0.0	0.067	0.030	0.036	0.036	0.242±0.076	0.106	-0.027±0.118	0.056
0.25	4.00	3.59	0.095±0.113	0.074	0.0	0.055	0.023	0.029	0.033	0.174±0.094	0.102	0.097±0.162	0.063
0.25	5.00	3.98	-0.004±0.085	0.066	0.0	0.049	0.018	0.025	0.031	0.096±0.071	0.093	0.130±0.127	0.058
0.33	1.50	1.97	0.475±0.218	0.284	0.0	0.244	0.071	0.117	0.048	0.489±0.170	0.394	-0.006±0.281	0.233
0.33	2.00	2.21	0.121±0.073	0.095	0.0	0.075	0.034	0.040	0.026	0.173±0.062	0.129	0.034±0.098	0.075
0.33	2.50	2.43	0.079±0.102	0.109	0.0	0.095	0.021	0.043	0.026	0.029±0.103	0.128	-0.149±0.136	0.072
0.33	3.00	2.62	0.177±0.058	0.071	0.0	0.051	0.028	0.029	0.027	0.242±0.049	0.090	0.061±0.079	0.049
0.33	4.00	2.98	0.042±0.059	0.060	0.0	0.044	0.023	0.025	0.022	0.217±0.062	0.088	0.180±0.098	0.053
0.33	5.00	3.30	0.041±0.086	0.066	0.0	0.053	0.018	0.026	0.022	0.307±0.092	0.112	0.282±0.156	0.077
0.33	6.00	3.59	0.687±0.346	0.073	0.0	0.0	0.056	0.026	0.038	0.069±0.153	0.045	-0.600±0.263	0.134
0.33	7.00	3.86	0.365±0.339	0.058	0.0	0.0	0.045	0.022	0.031	0.062±0.188	0.046	-0.309±0.316	0.076
0.40	2.00	1.97	0.140±0.085	0.109	0.0	0.088	0.038	0.047	0.023	0.238±0.077	0.156	0.093±0.125	0.096
0.40	3.00	2.32	0.078±0.054	0.064	0.0	0.048	0.027	0.028	0.019	0.137±0.044	0.083	0.055±0.073	0.047
0.40	4.00	2.62	0.193±0.071	0.071	0.0	0.053	0.029	0.031	0.021	0.195±0.054	0.087	-0.000±0.088	0.049
0.40	5.00	2.89	0.106±0.064	0.054	0.004	0.037	0.024	0.024	0.019	0.169±0.055	0.065	0.060±0.090	0.035
0.40	6.00	3.14	0.011±0.058	0.047	0.005	0.034	0.018	0.021	0.017	0.143±0.049	0.066	0.140±0.085	0.040
0.40	7.00	3.37	0.040±0.091	0.048	0.032	0.0	0.024	0.020	0.016	0.166±0.075	0.047	0.131±0.127	0.045
0.40	8.00	3.59	0.106±0.104	0.052	0.033	0.0	0.028	0.022	0.019	0.151±0.074	0.046	0.015±0.127	0.041
0.40	9.00	3.79	0.178±0.208	0.046	0.0	0.0	0.036	0.020	0.019	0.110±0.147	0.044	-0.065±0.248	0.011
0.50	3.00	1.97	0.074±0.060	0.073	0.0	0.057	0.029	0.032	0.014	0.125±0.050	0.094	0.042±0.083	0.057
0.50	4.00	2.21	0.190±0.074	0.067	0.0	0.048	0.032	0.031	0.015	0.181±0.056	0.083	0.002±0.096	0.047
0.50	5.00	2.42	0.183±0.079	0.056	0.006	0.037	0.027	0.028	0.015	0.243±0.064	0.068	0.061±0.106	0.041
0.50	6.00	2.62	0.085±0.062	0.047	0.001	0.032	0.022	0.024	0.012	0.209±0.055	0.066	0.125±0.091	0.040
0.50	7.00	2.81	0.086±0.067	0.048	0.018	0.031	0.019	0.023	0.013	0.176±0.055	0.064	0.094±0.092	0.039
0.50	8.00	2.98	0.040±0.087	0.032	0.007	0.0	0.019	0.021	0.012	0.243±0.081	0.040	0.201±0.134	0.048
0.50	10.00	3.30	0.217±0.130	0.052	0.032	0.0	0.032	0.022	0.013	0.138±0.086	0.044	-0.013±0.158	0.023
0.50	12.00	3.59	0.184±0.150	0.040	0.0	0.0	0.031	0.023	0.013	0.170±0.119	0.040	0.004±0.194	0.033
0.60	5.00	2.05	0.231±0.100	0.058	0.026	0.026	0.031	0.031	0.011	0.058±0.061	0.046	-0.176±0.104	0.042
0.60	6.00	2.21	0.240±0.083	0.057	0.002	0.039	0.026	0.030	0.012	0.108±0.055	0.052	-0.134±0.094	0.036
0.60	7.00	2.36	0.091±0.061	0.050	0.005	0.037	0.019	0.025	0.010	0.110±0.049	0.061	0.020±0.082	0.036
0.60	8.00	2.49	0.149±0.088	0.033	0.006	0.0	0.020	0.024	0.009	0.163±0.072	0.035	0.032±0.114	0.044
0.60	10.00	2.75	0.109±0.081	0.028	0.003	0.0	0.010	0.025	0.008	0.119±0.070	0.029	0.017±0.107	0.046
0.60	12.00	2.98	0.001±0.120	0.030	0.0	0.0	0.022	0.019	0.007	0.120±0.109	0.034	0.127±0.171	0.052
0.60	14.00	3.20	0.034±0.116	0.030	0.0	0.0	0.020	0.021	0.007	0.053±0.099	0.029	0.024±0.155	0.038
0.67	6.00	1.97	0.238±0.130	0.047	0.001	0.019	0.023	0.034	0.009	0.063±0.082	0.037	-0.148±0.146	0.054
0.67	7.00	2.09	0.182±0.081	0.052	0.001	0.037	0.020	0.030	0.008	0.084±0.058	0.047	-0.076±0.101	0.035
0.67	8.00	2.21	0.244±0.093	0.048	0.031	0.0	0.020	0.029	0.007	0.035±0.058	0.032	-0.200±0.097	0.045
0.67	10.00	2.42	0.107±0.088	0.030	0.006	0.0	0.011	0.026	0.008	0.082±0.071	0.028	-0.030±0.110	0.040
0.67	12.00	2.62	-0.016±0.091	0.035	0.023	0.0	0.016	0.020	0.005	0.073±0.080	0.035	0.087±0.126	0.014
0.67	14.00	2.81	0.058±0.111	0.029	0.0	0.0	0.017	0.022	0.005	0.176±0.103	0.032	0.114±0.158	0.051
0.67	16.00	2.98	0.351±0.284	0.036	0.0	0.0	0.002	0.036	0.007	-0.005±0.168	0.026	-0.345±0.263	0.085
0.75	8.00	1.88	0.215±0.187	0.043	0.002	0.0	0.008	0.042	0.006	0.378±0.198	0.053	0.211±0.338	0.135
0.75	9.00	1.97	0.165±0.108	0.033	0.002	0.0	0.003	0.033	0.005	0.122±0.086	0.031	-0.021±0.147	0.057
0.75	10.00	2.05	0.189±0.108	0.033	0.007	0.0	0.015	0.028	0.005	0.071±0.077	0.030	-0.112±0.130	0.044
0.75	12.00	2.21	0.108±0.103	0.035	0.019	0.0	0.015	0.024	0.004	0.098±0.080	0.033	0.007±0.133	0.016
0.75	14.00	2.36	0.100±0.115	0.028	0.0	0.0	0.016	0.023	0.004	0.153±0.101	0.030	0.052±0.155	0.054
0.75	16.00	2.49	0.132±0.114	0.028	0.0	0.0	0.010	0.026	0.004	0.267±0.107	0.032	0.128±0.166	0.057
0.80	12.00	1.97	0.022±0.138	0.026	0.008	0.0	0.009	0.023	0.003	0.152±0.127	0.030	0.140±0.210	0.035
0.80	14.00	2.09	0.077±0.139	0.027	0.0	0.0	0.003	0.025	0.003	0.030±0.109	0.025	-0.064±0.166	0.042
0.80	16.00	2.21	0.142±0.124	0.028	0.0	0.0	0.005	0.028	0.003	0.165±0.104	0.028	-0.014±0.160	0.043

2722C26

which we find to be consistent with our overall results, then $R_n = R_d$ and $R_n = R_p$. In this manner we can compare R_p, R_d, and R_n, independent of the assumptions about R_n needed to calculate σ_n from σ_d and σ_p in the impulse approximation.

At each of the 75 kinematic points (ν, Q^2), the quantity δ was extracted as one of the two parameters of a least square fit of the form of Eq. (III. 2) to interpolated values of σ_d/σ_p versus ϵ'. The interpolations program was almost identical to the one used to interpolate Σ. At each (ν, Q^2) point, the value of R_p in $\epsilon' = \epsilon/(1 + \epsilon R_p)$ was taken to be that listed in Table 1. Values of δ and its random error from these fits are reproduced in Table 1 along with estimates of the total systematic uncertainty $\Delta\delta$. One contribution to this uncertainty arose from the ambiguity in the appropriate choice of R_p used to calculate ϵ' and ranged from 0. 0 to 0. 20 in δ. Another uncertainty arose from the uncertainty of 1. 3% in the ratio of deuteron to proton normalization factors N^d_{AB}/N^p_{AB} and ranged from 0. 01 to 0. 12 in δ. A third uncertainty in δ arose from taking the normalization factor N^d_{AC} to be equal to N^p_{AC}, which had been calculated by a comparison of elastic e-p cross sections; this uncertainty ranged from 0. 02 to 0. 23 in δ. The quadratic sum of these three uncertainties is presented as $\Delta\delta$ in Table 1. In general, the systematic uncertainty in δ is much smaller than the random error.

The result $\delta = 0$ is consistent with all the data listed in Table 1. Values of δ are typically less than one standard deviation, and in only two instances more than two standard deviations, different from zero. Weighted averages of δ for each of the 11 values of x are presented in Figure 8 along with their statistical errors. Systematic uncertainties in these averages range from 0. 03 to 0. 08 and are largest in the range $0.15 \leq x \leq 0.33$. No statistically significant

deviation from zero can be seen anywhere in these data. When the normalization factor N^d_{AC} was taken to be unity instead of 1.019, the average values of δ in the range $0.10 \leq x \leq 0.50$ were all within one standard deviation of zero. The average value of δ over the full x-Q^2 array, $\bar{\delta} = 0.031 \pm 0.015$, has a total systematic uncertainty of $\Delta\bar{\delta} = 0.036$ and is consistent with zero. If δ is calculated using only cross sections from experiments A and B, its average over the restricted x-Q^2 array is $\bar{\delta} = -0.001 \pm 0.022$. The only hint of some nonzero behavior of δ occurs for $W \lesssim 2.5$ GeV and $x \geq 0.60$, where R_d is consistently smaller than R_p. Although the effect is not statistically significant, on the two standard deviation level, this behavior is consistent with a vanishing[15] R_n at low W. Present estimates of the off-mass-shell corrections to the deuteron smearing ratios[11,13,16] are much smaller than the errors in R_d and cannot explain this effect. Except for this possible difference at low W, we conclude that $R_d = R_p$, and hence that $R_n = R_p$, over the full range of the x-Q^2 array.

B. Kinematic Variation of R_p

The behavior of R_p in the Bjorken limit is an important test of constituent models[17,18] of nucleon structure. In conventional field theories with only spin-$\frac{1}{2}$ charged constituents, R_p should vanish as $1/Q^2$ in the Bjorken limit.[18,19] More recently, field theories with asymptotic freedom[20,21] predict that R_p should vanish as $1/\log Q^2$. In both cases, the presence of charged spin-0 constituents would be reflected in a nonvanishing contribution[22] to R_p. The kinematic variation of R_p was, however, difficult to ascertain because of large statistical errors and systematic uncertainties in the present data. Consequently, two approaches to the study of the kinematic variation of R_p were used. In the first approach, universal fits were made to the entire body of data for R_p listed

in Table 1. In the second approach, individual fits to R_p were attempted at each of the 11 values of x at which this quantity was available. The interpretation of these fits is discussed in this section.

The results of four least square fits to all the data for R_p are presented in Table 2. Systematic uncertainties in the fit parameters arising from the five uncertainties in R_p were added in quadrature to produce the numbers listed under Δ in Table 2. When only the R_p data for $W \geq 2.0$ GeV were used in these fits, the best fit parameters shifted by less than one standard deviation.

TABLE 2

Universal fits to R_p. The best-fit parameters for each fit function are listed along with the total χ^2 of the fit (75 data points). The quantity Δ represents the systematic uncertainty in each parameter.

Fit Function	Best-fit Parameter	Δ	χ^2
$R_p = c$	$c = 0.138 \pm 0.011$	0.056	71
$R_p = g(x)\frac{Q^2}{\nu^2}$	$c = 0.392 \pm 0.100$	0.152	63
$g(x) = c + \frac{d}{x^2}$	$d = 0.073 \pm 0.012$	0.041	
$R_p = \frac{cQ^2}{(Q^2+d^2)^2}$	$c = 0.861 \pm 0.202$*	0.363*	62
	$d^2 = 0.988 \pm 0.388$*	0.229*	
$R_p = \frac{c}{1+d \ln \frac{Q^2}{M^2}}$	$c = 0.294 \pm 0.063$	0.165	58
	$d = 0.808 \pm 0.358$	0.237	

* in units of GeV^2

In addition to the fits listed in Table 2, fits of the forms $R_p = cQ^2$, $R_p = cQ^2(1-x)^2$, $R_p = Q^2/\nu^2$, $R_p = cQ^2/\nu^2$ were attempted. These functions

provided very poor fits to the data, and are consequently not listed. Except at low $x \lesssim 0.2$, the data for R_p are inconsistent with a linear rise in Q^2, as required by simple vector dominance models[23] of inelastic e-N scattering. A constant value still fits the R_p data quite well. The best-fit value $R_p = 0.138$ is consistent with the values $R_p = 0.16 \pm 0.10$ and $R_p = 0.18 \pm 0.10$ reported in earlier measurements[3,7] of this quantity over different kinematic ranges. The strict Callan-Cross relation $R_p = Q^2/\nu^2$ fits the data very poorly, and the form $R_p = cQ^2/\nu^2$ is only marginally better. However, a more general spin-$\frac{1}{2}$ prediction $R_p = g(x)Q^2/\nu^2$ provides an excellent representation of the R_p data. Such a deviation from simple Q^2/ν^2 behavior at large ω has been predicted from Regge arguments[22] in the framework of light-cone algebras,[19] and deduced[24] from ρ-electroproduction data.[25] The fit function[26] $R_p = cQ^2/(Q^2+d^2)^2$ insures that $R_p \to 0$ as $Q^2 \to 0$, as required by gauge invariance, and vanishes as $1/Q^2$ in the Bjorken limit. It provides excellent fits to the data. A similar[26] $R_p = cQ^2/(Q^2+d^2)$, that vanishes as $Q^2 \to 0$ and approaches a nonzero constant in the Bjorken limit, fits the proton data with equally good χ^2. However, the best fit value of d^2 is negative, producing a singularity in R_p at $Q^2 = -d^2$, and the fit is not included in the table. The final fit is derived from $R_p = \frac{\alpha^2}{\ln(Q^2/\beta^2)}$, with $d = \left(\ln\frac{M^2}{\beta^2}\right)^{-1}$ and $c = \alpha^2 d$, and is necessarily singular at $Q^2 = \beta^2 = 0.255\ \mathrm{GeV}^2$. This function fits the data equally as well as $R_p = cQ^2/(Q^2+d^2)^2$, and the present data cannot distinguish between a $1/Q^2$ and $1/\log Q^2$ behavior of R_p in the Bjorken limit. Although these two functional forms fit the data better than the constant fit, we cannot rule out a nonvanishing contribution to R_p, at least not on the basis of the universal fits to all the present data. For a sample of data restricted to $x \geq 0.25$, the constant, the $1/Q^2$, and the $1/\log Q^2$ functions fit R_p equally well.

The x-Q^2 array facilitated a study of the Q^2-dependence of R_p for fixed values of x in the range $0.1 \leq x \leq 0.8$. This approach allowed unbiased tests of functional forms that would have had difficulty modeling any overall x-dependence of R_p. It consequently allowed more detailed tests of the behavior of R_p in the Bjorken limit. The data for R_p are plotted versus Q^2 in Figure 9 for the 11 fixed values of x available; the corresponding data for R_d are also plotted for comparison. The three curves plotted at each x in these figures represent the best fits of the functional forms $R = c(x)$, $R = \alpha^2(x)/\log(Q^2/\beta^2)$, and $R = c(x)Q^2/(Q^2+d^2)^2$, corresponding to three of the universal fits reported in Table 2. The two parameters β^2 and d^2 were set equal to the corresponding parameters of the universal fits in Table 2. The total χ^2 for the 11 fixed-x fits to R_p (64 degrees of freedom) was 55 for the constant fit, 51 for the modified $1/Q^2$ fit, and 47 for the $1/\log Q^2$ fit. Fixed-x fits of other functional forms not shown in these figures were also attempted. In particular, a form $R = c(x)/Q^2$ fits the R_p data well for $x \geq 0.25$, but has less than 20% confidence for $x \leq 0.2$. The form $R_p = c(x)Q^2$ is consistent with the data for $x \leq 0.2$, but is a very poor fit at higher x. Over the full range of x, it is difficult to distinguish, on the basis of χ^2, among the three functional forms plotted. The relatively larger values of χ^2 obtained in the constant universal fit can be seen as the result of a slow variation of R_p with x, which varies from about 0.3 at low values of x to about 0.1 at the high values of x reported. On the other hand, the success of the universal $1/\log Q^2$ fit can be attributed to the fact that it (perhaps fortuitously) models this x-variation of R_p quite well. The modified $1/Q^2$ universal fit also models the low-x, low-Q^2 behavior of R_p fairly well and provides almost as good a fit as $1/\log Q^2$ to all the data. In summary, the present data for R_p are consistent with either a constant, a $1/Q^2$, or a $1/\log Q^2$ dependence

in the Bjorken limit. The present errors on R_p do not allow us to distinguish among these three functional forms.

The x-Q^2 array also facilitated a study of the kinematic variation of νR_p for fixed values of x. Light-cone algebras with only spin-$\frac{1}{2}$ charged constituents predict[18,19] that νR_p should scale, i.e., $\nu R_p(x,Q^2) = a(x)$. If there are charged spin-0 partons in the proton,[22] then $\nu R_p(x,Q^2) = a(x) + \nu b(x)$, where b(x) is the ratio of spin-0 to spin-$\frac{1}{2}$ contributions to νW_2^p, in the limit of large Q^2. Other non-spin-$\frac{1}{2}$ contributions[24] to νW_2^p would result in a nonzero value of b(x), which would also be expected in asymptotically free field theories.[21] In Fig. 10, νR_p is plotted versus Q^2 for fixed values of x between 0.1 and 0.8. The solid lines represent least-square fits of the form $\nu R_p = a + b\nu = a + \frac{b}{2Mx}Q^2$. Best fit values of b(x) and its random errors are presented in Table 3 for the eleven values of x studied. The five contributions to the

TABLE 3

Best-fit parameters b and their random errors and systematic uncertainties from least-square fits of the form $\nu R_p = a + b\nu$.

x	b	Δb
0.10	0.679 ± 0.330	0.130
0.15	0.278 ± 0.166	0.111
0.20	0.118 ± 0.090	0.058
0.25	0.014 ± 0.084	0.033
0.33	0.003 ± 0.098	0.030
0.40	0.055 ± 0.066	0.032
0.50	0.123 ± 0.075	0.034
0.60	- 0.087 ± 0.123	0.036
0.67	- 0.111 ± 0.148	0.049
0.75	0.009 ± 0.221	0.031
0.80	0.496 ± 0.642	0.049

systematic uncertainty in R_p also give uncertainties in the parameter b. The quadratic sum of the five such uncertainties is reported in Table 3 as Δb, the systematic uncertainty in b. When the above fits were restricted to $W \geq 2.0$ GeV, the best-fit parameters shifted by less than one standard deviation, except at $x = 0.5$, where b shifted from 0.123 ± 0.075 to 0.023 ± 0.114. When fits were made to the R_p data from the x-Q^2 array restricted to experiments A and B, the results for b agreed with those of Table 3 within their random errors. For $0.25 \leq x \leq 0.80$, b is small and consistent with zero, within the random errors quoted. The average value of b over this range of x is $\bar{b} = 0.035 \pm 0.036$, with an estimated systematic uncertainty of 0.033. The present results are consistent with scaling of νR_p in this range, indicative of purely spin-$\frac{1}{2}$ constituents, in a parton model of the proton. However, they are also consistent with about a 10% spin-0 contribution to νW_2^p, which would lead to a nonvanishing value of R_p in the Bjorken limit.[22] Asymptotically free field theories[20] are also consistent with these results, as they predict[21] a small increment above exact scaling behavior for νR_p. Large values of b are encountered for $x \lesssim 0.2$, but a considerable portion of the data at these values of x is for $Q^2 \leq 2.0$ GeV^2, and the observed slope in νR_p may represent only the low-Q^2 turnon[27] of νW_2^p. In conclusion, the present data for νR_p are consistent with scaling, but the data are not accurate enough to rule out about a 10% deviation from exact scaling.

C. Separation of the Structure Functions

At each kinematic point of the x-Q^2 array, the quantities $2MW_1$ and νW_2 were derived from σ_L and σ_T according to Eq. (I.3). The separated values of $F_1(x,Q^2) = 2MW_1(x,Q^2)$ and $F_2(x,Q^2) = \nu W_2(x,Q^2)$ are reported in Table 4,

along with the random errors and relative systematic uncertainties in these quantities. Plots of $F_1(x,Q^2)$ and $F_2(x,Q^2)$ versus Q^2 for selected fixed values of x are presented in Figs. 11 and 12 for both the proton and deuteron. The random errors in F_1 and F_2 were computed from the error matrix of the least-square fit to Σ, and therefore include a contribution from the random error in R at each point. As most of our cross section data were measured at values of ϵ between 0.6 and 0.9, this contribution is, in general, much larger for F_1 (corresponding to $\epsilon = 0$) than for F_2 (corresponding to $\epsilon = 1$). The relative uncertainties, which arise from the uncertainties in the normalization factors and from the relative cross section uncertainties mentioned earlier, are those which can affect the Q^2-dependence of F_1 and F_2. They were estimated in a manner similar to that used to estimate the uncertainties in R, and were added in quadrature to produce the numbers listed under Δ in Table 4. The relative uncertainty arising from the uncertainty in the radiative corrections ranged from 2% to 10% in F_1 and from 1.5% to 2% in F_2. Overall normalization uncertainties in F_1 and F_2 are estimated to be 3.4% for the proton structure functions and 3.6% for the deuteron.

D. Tests of Structure Function Scaling

In the ranges of ν and Q^2 available from the present experiments, tests of structure function scaling are dependent upon the choice of scaling variable. Bjorken's original hypothesis[28] was that $2MW_1(\nu, Q^2)$ and $\nu W_2(\nu, Q^2)$ would scale in the variable $\omega = 2M\nu/Q^2$ (i.e., become functions only of ω) in the limit $\nu \to \infty$ $Q^2 \to \infty$, with ν/Q^2 held fixed. Within the experimental errors, the early data[7] for νW_2^p were consistent with scaling in ω for $Q^2 \geq 1$ GeV^2 and $W \geq 2.6$ GeV. Other scaling variables, all of which approach ω as $Q^2 \to \infty$,

TABLE 4

Separated values of $F_1 = 2MW_1$ and $F_2 = \nu W_2$ for the proton and deuteron, with random errors and relative systematic uncertainties Δ.

x	Q^2	$2MW_1^p$	Δ	νW_2^p	Δ	$2MW_1^d$	Δ	νW_2^d	Δ
0.10	1.00	2.7320±0.2435	0.2168	0.3100±0.0086	0.0088	5.3689±0.3524	0.4173	0.5808±0.0126	0.0206
0.10	1.25	2.5293±0.2333	0.2083	0.3291±0.0095	0.0092	5.3258±0.4165	0.4067	0.6120±0.0154	0.0205
0.10	1.50	2.6576±0.1983	0.2238	0.3381±0.0093	0.0095	5.0837±0.3422	0.4125	0.6402±0.0145	0.0215
0.10	2.00	2.5390±0.2401	0.2242	0.3598±0.0172	0.0099	5.1486±0.3443	0.4315	0.6441±0.0248	0.0225
0.10	2.50	2.3170±0.6479	0.2683	0.4295±0.0737	0.0193	5.2006±0.9577	0.5660	0.6649±0.1090	0.0451
0.15	1.00	1.6898±0.1661	0.1565	0.3308±0.0062	0.0098	2.9340±0.2830	0.2900	0.6032±0.0093	0.0217
0.15	1.25	1.9501±0.1395	0.1574	0.3315±0.0074	0.0101	3.1496±0.1921	0.2917	0.6118±0.0103	0.0230
0.15	1.50	2.1034±0.1369	0.1514	0.3283±0.0068	0.0096	3.2092±0.2393	0.2555	0.6216±0.0101	0.0219
0.15	2.00	1.8090±0.0937	0.1404	0.3448±0.0089	0.0102	2.9493±0.2033	0.2427	0.6459±0.0132	0.0236
0.15	2.50	1.7987±0.1546	0.1513	0.3617±0.0162	0.0143	3.0912±0.2153	0.2792	0.6613±0.0223	0.0330
0.15	3.00	1.8201±0.1803	0.1502	0.3544±0.0249	0.0146	3.5006±0.2277	0.2940	0.6407±0.0336	0.0345
0.15	3.50	1.9293±0.2252	0.1548	0.3321±0.0277	0.0147	3.4415±0.2787	0.2923	0.6649±0.0357	0.0369
0.20	1.00	1.5845±0.1287	0.1575	0.3183±0.0049	0.0089	2.7658±0.1911	0.3209	0.5720±0.0073	0.0197
0.20	1.25	1.4686±0.1173	0.1416	0.3288±0.0061	0.0097	2.5827±0.1845	0.2822	0.5880±0.0085	0.0213
0.20	1.50	1.2762±0.1070	0.1205	0.3399±0.0056	0.0098	2.2135±0.1557	0.2356	0.6000±0.0076	0.0212
0.20	2.00	1.4645±0.0710	0.1029	0.3333±0.0058	0.0093	2.4341±0.1128	0.1784	0.6076±0.0077	0.0205
0.20	2.50	1.6122±0.0776	0.1067	0.3270±0.0076	0.0098	2.5299±0.1466	0.1873	0.5986±0.0108	0.0221
0.20	3.00	1.5177±0.0948	0.1086	0.3394±0.0124	0.0124	2.5064±0.1276	0.1996	0.6113±0.0169	0.0277
0.20	3.50	1.4257±0.1150	0.1036	0.3457±0.0171	0.0132	2.2603±0.1571	0.1900	0.6367±0.0236	0.0303
0.20	4.00	1.4912±0.0967	0.1021	0.3247±0.0156	0.0130	2.2965±0.1345	0.1844	0.6385±0.0218	0.0312
0.25	1.00	1.0798±0.1275	0.1642	0.3184±0.0046	0.0087	1.8854±0.1832	0.3399	0.5509±0.0066	0.0186
0.25	1.25	1.3236±0.1200	0.1303	0.3112±0.0046	0.0088	2.1859±0.1662	0.2872	0.5500±0.0067	0.0191
0.25	1.50	1.1183±0.0962	0.1162	0.3188±0.0042	0.0088	1.8561±0.1320	0.2364	0.5575±0.0058	0.0189
0.25	2.00	1.1714±0.0662	0.0858	0.3253±0.0047	0.0087	1.8545±0.0985	0.1508	0.5623±0.0063	0.0184
0.25	2.50	1.1623±0.0920	0.0872	0.3195±0.0072	0.0095	1.8625±0.1642	0.1633	0.5634±0.0100	0.0206
0.25	3.00	1.1688±0.0612	0.0787	0.3211±0.0086	0.0100	1.9217±0.0848	0.1339	0.5559±0.0113	0.0207
0.25	4.00	1.1873±0.0792	0.0720	0.3082±0.0129	0.0100	1.9741±0.1030	0.1325	0.5493±0.0176	0.0223
0.25	5.00	1.2402±0.0653	0.0716	0.2959±0.0112	0.0103	2.0184±0.0838	0.1273	0.5295±0.0142	0.0236
0.33	1.50	0.7480±0.1035	0.1193	0.2916±0.0038	0.0079	1.2260±0.1298	0.2470	0.4827±0.0053	0.0163
0.33	2.00	0.8939±0.0505	0.0677	0.2794±0.0033	0.0071	1.4293±0.0659	0.1277	0.4676±0.0046	0.0146
0.33	2.50	0.8863±0.0734	0.0740	0.2756±0.0043	0.0076	1.5366±0.1389	0.1451	0.4559±0.0062	0.0157
0.33	3.00	0.8064±0.0316	0.0467	0.2799±0.0039	0.0070	1.2626±0.0401	0.0777	0.4622±0.0051	0.0145
0.33	4.00	0.8449±0.0331	0.0449	0.2674±0.0057	0.0072	1.2266±0.0442	0.0733	0.4534±0.0080	0.0146
0.33	5.00	0.8084±0.0452	0.0435	0.2600±0.0080	0.0078	1.1362±0.0569	0.0750	0.4590±0.0106	0.0164
0.33	6.00	0.5898±0.0765	0.0312	0.3114±0.0243	0.0069	1.2554±0.0927	0.0603	0.4201±0.0301	0.0092
0.33	7.00	0.6487±0.0857	0.0323	0.2795±0.0336	0.0063	1.2306±0.1015	0.0588	0.4124±0.0401	0.0094
0.40	2.00	0.6927±0.0464	0.0578	0.2464±0.0028	0.0062	1.0314±0.0573	0.1054	0.3985±0.0038	0.0118
0.40	3.00	0.6342±0.0250	0.0356	0.2303±0.0032	0.0055	0.9751±0.0299	0.0594	0.3732±0.0042	0.0109
0.40	4.00	0.5570±0.0252	0.0309	0.2331±0.0041	0.0057	0.8831±0.0302	0.0516	0.3700±0.0054	0.0117
0.40	5.00	0.5683±0.0229	0.0272	0.2259±0.0049	0.0054	0.8589±0.0277	0.0433	0.3610±0.0062	0.0097
0.40	6.00	0.5731±0.0228	0.0259	0.2118±0.0044	0.0052	0.8422±0.0257	0.0421	0.3521±0.0054	0.0099
0.40	7.00	0.5430±0.0280	0.0238	0.2001±0.0082	0.0056	0.8108±0.0314	0.0358	0.3501±0.0098	0.0079
0.40	8.00	0.4982±0.0261	0.0218	0.2170±0.0088	0.0058	0.7907±0.0290	0.0343	0.3399±0.0105	0.0079
0.40	9.00	0.4746±0.0401	0.0205	0.2104±0.0202	0.0048	0.7868±0.0476	0.0335	0.3289±0.0246	0.0074
0.50	3.00	0.4129±0.0194	0.0248	0.1714±0.0021	0.0040	0.6160±0.0228	0.0417	0.2679±0.0028	0.0075
0.50	4.00	0.3439±0.0167	0.0182	0.1677±0.0028	0.0037	0.5286±0.0188	0.0302	0.2558±0.0038	0.0072
0.50	5.00	0.3166±0.0164	0.0153	0.1593±0.0029	0.0033	0.4644±0.0183	0.0236	0.2454±0.0036	0.0056
0.50	6.00	0.3181±0.0134	0.0136	0.1505±0.0027	0.0033	0.4516±0.0156	0.0217	0.2380±0.0034	0.0060
0.50	7.00	0.3014±0.0136	0.0135	0.1453±0.0029	0.0031	0.4365±0.0150	0.0210	0.2279±0.0033	0.0055
0.50	8.00	0.2974±0.0159	0.0115	0.1392±0.0047	0.0026	0.4080±0.0176	0.0163	0.2285±0.0056	0.0042
0.50	10.00	0.2555±0.0160	0.0112	0.1429±0.0067	0.0030	0.4063±0.0174	0.0163	0.2124±0.0075	0.0045
0.50	12.00	0.2501±0.0173	0.0095	0.1379±0.0083	0.0033	0.3823±0.0205	0.0143	0.2084±0.0104	0.0048
0.60	5.00	0.1736±0.0114	0.0082	0.1023±0.0018	0.0020	0.2902±0.0130	0.0126	0.1470±0.0023	0.0028
0.60	6.00	0.1601±0.0085	0.0072	0.0983±0.0018	0.0020	0.2542±0.0094	0.0111	0.1395±0.0021	0.0030
0.60	7.00	0.1624±0.0070	0.0068	0.0900±0.0015	0.0020	0.2338±0.0078	0.0100	0.1319±0.0017	0.0033
0.60	8.00	0.1484±0.0081	0.0055	0.0884±0.0022	0.0017	0.2142±0.0093	0.0073	0.1290±0.0026	0.0024
0.60	10.00	0.1370±0.0068	0.0047	0.0809±0.0021	0.0016	0.1994±0.0083	0.0067	0.1188±0.0027	0.0022
0.60	12.00	0.1335±0.0081	0.0045	0.0726±0.0046	0.0016	0.1882±0.0097	0.0064	0.1144±0.0056	0.0024
0.60	14.00	0.1252±0.0072	0.0042	0.0712±0.0041	0.0016	0.1807±0.0088	0.0057	0.1047±0.0050	0.0022
0.67	6.00	0.0997±0.0085	0.0042	0.0653±0.0014	0.0012	0.1651±0.0099	0.0065	0.0929±0.0018	0.0017
0.67	7.00	0.0937±0.0051	0.0039	0.0604±0.0011	0.0012	0.1469±0.0060	0.0059	0.0868±0.0013	0.0018
0.67	8.00	0.0861±0.0048	0.0031	0.0597±0.0013	0.0013	0.1392±0.0054	0.0046	0.0804±0.0015	0.0015
0.67	10.00	0.0813±0.0044	0.0028	0.0519±0.0015	0.0009	0.1182±0.0052	0.0039	0.0737±0.0017	0.0013
0.67	12.00	0.0784±0.0043	0.0029	0.0455±0.0019	0.0008	0.1069±0.0050	0.0037	0.0677±0.0021	0.0012
0.67	14.00	0.0699±0.0040	0.0022	0.0444±0.0022	0.0009	0.0960±0.0048	0.0030	0.0677±0.0027	0.0014
0.67	16.00	0.0573±0.0074	0.0018	0.0470±0.0039	0.0010	0.0980±0.0090	0.0029	0.0592±0.0047	0.0012
0.75	8.00	0.0411±0.0051	0.0016	0.0300±0.0010	0.0006	0.0537±0.0064	0.0022	0.0445±0.0012	0.0008
0.75	9.00	0.0389±0.0028	0.0013	0.0279±0.0006	0.0005	0.0580±0.0034	0.0019	0.0400±0.0008	0.0007
0.75	10.00	0.0359±0.0024	0.0012	0.0267±0.0008	0.0005	0.0550±0.0028	0.0018	0.0369±0.0009	0.0006
0.75	12.00	0.0332±0.0020	0.0012	0.0237±0.0009	0.0004	0.0480±0.0023	0.0016	0.0339±0.0009	0.0006
0.75	14.00	0.0294±0.0018	0.0009	0.0213±0.0010	0.0004	0.0415±0.0022	0.0012	0.0314±0.0012	0.0006
0.75	16.00	0.0264±0.0016	0.0008	0.0199±0.0009	0.0004	0.0361±0.0019	0.0011	0.0305±0.0011	0.0006
0.80	12.00	0.0194±0.0018	0.0006	0.0133±0.0006	0.0002	0.0263±0.0020	0.0008	0.0204±0.0007	0.0003
0.80	14.00	0.0169±0.0014	0.0005	0.0125±0.0006	0.0002	0.0252±0.0016	0.0007	0.0179±0.0008	0.0003
0.80	16.00	0.0145±0.0010	0.0004	0.0116±0.0005	0.0002	0.0212±0.0012	0.0006	0.0173±0.0006	0.0003

2722C25

have been proposed, and must be considered on an equal footing with ω at present values of Q^2. In the earlier inelastic e-p measurements,[7] use of the scaling variable $\omega' = \omega + M^2/Q^2 = 1 + W^2/Q^2$ extended the range of W for which scaling of νW_2^p was valid down to W = 1.8 GeV. The variable later gained some theoretical justification on the basis of finite energy sum rules[29] and dimensional considerations.[30] The variable $\omega_L = M/((Q^2+\nu^2)^{\frac{1}{2}}-\nu)$ has been suggested[31] as the scaling variable appropriate to light-cone algebras. Use of a phenomenological scaling variable[32] $\omega_W = \frac{2M\nu + a^2}{Q^2 + b^2}$ (where a^2 and b^2 are fit parameters) extends scaling down to the photoproduction limit $Q^2 = 0$. The scaling variable $\omega_s = \omega + M_s^2/Q^2$, where $M_s^2 = 1.42$ GeV^2, has been used[33] to fit recent data for $2MW_1^p$ measured at scattering angles of 50 and 60 degrees with the SLAC 1.6 GeV Spectrometer. For the sake of brevity, we confine ourselves to tests of scaling in the two scaling variables ω and ω'. Previous scaling tests[4,12] based upon portions of the present experimental data are consistent with the present results. However, the statistical accuracy is much improved in the present work, permitting much more definitive tests of structure function scaling.

The two independent structure functions $F_1 = 2MW_1(x,Q^2)$ and $F_2 = \nu W_2(x,Q^2)$ as given in Table 4 were used in the present scaling tests. Evidence of a decrease with Q^2 for fixed $x = 1/\omega$ is readily apparent for both F_1 and F_2, at least for $x \gtrsim 0.3$. These separated data allowed tests of scaling of both structure functions, independent of any assumptions about the Q^2-dependence of R. Only the results for the proton structure functions are presented in any detail, as they do not suffer from any of the uncertainties of deuteron smearing corrections,[11] and are fully understood at present. Only data for $W \geq 2.0$ GeV and $Q^2 \geq 2.0$ GeV^2 were used in these scaling tests. These restrictions insured

that our tests were influenced neither by the prominent electroproduction resonances nor by the low-Q^2 turnon[27] of νW_2.

We tested scaling in the variables $\xi = \omega$ and $\xi = \omega'$ by fitting functions of the form $F_i(x,Q^2) = f_i(\xi)h_i(Q^2)$ to the data for F_1 and F_2. Here $f_1(\xi) = \xi\Sigma p_{1n}(1-1/\xi)^n$ and $f_2(\xi) = \Sigma p_{2n}(1-1/\xi)^n$, where n ranges from 3 to 7. Three forms for $h_i(Q^2)$ were tested: a constant $h_i(Q^2) = 1$ for exact scaling; the scale-breaking form $h_i(Q^2) = 1 - 2Q^2/\Lambda_i^2$ suggested by constituent models[34] wherein $1/\Lambda^2$ is the parton "size"; and the propagator form[35,36] $h_i(Q^2) = (1+Q^2/\Lambda_i^2)^{-2}$. Best fit values for Λ_i^2 and for the polynomial coefficients p_{in} were obtained simultaneously by least-square fits. Our studies indicated that the results for Λ_1^2 and Λ_2^2 were independent of the functional forms for $f_1(\xi)$ and $f_2(\xi)$. The fits provided a comparison of deviations from scaling of $2MW_1$ and νW_2; in particular, they permit unbiased tests of models[35] that predict a larger scaling violation for $2MW_1$ than for νW_2.

The best-fit parameters $1/\Lambda_1^2$ and $1/\Lambda_2^2$ of fits in the scaling variable $\xi = \omega$ are presented in Table 5. Systematic uncertainties in these quantities arise from the same effects that led to the relative uncertainties in F_1 and F_2 listed in Table 4. These systematic uncertainties were added in quadrature and included in the errors quoted. For $\xi = \omega$, the two scale-breaking forms listed in

TABLE 5

Deviations from scaling in ω, from least-square fits of the form $F_i(x,Q^2) = f_i(\omega)h_i(Q^2)$ to the proton data only.

x range	$h_i(Q^2) = 1 - 2Q^2/\Lambda_i^2$		$h_i(Q^2) = (1 + Q^2/\Lambda_i^2)^{-2}$	
	$1/\Lambda_1^2$	$1/\Lambda_2^2$	$1/\Lambda_1^2$	$1/\Lambda_2^2$
$0.1 \leq x \leq 0.8$	0.0144±0.0014	0.0141±0.0008	0.0225±0.0038	0.0204±0.0017
$0.3 \leq x \leq 0.8$	0.0147±0.0013	0.0144±0.0008	0.0245±0.0040	0.0213±0.0019

Table 5 provided much better fits than the exact scaling form $F_i(x,Q^2) = f_i(\omega)$. The χ^2 for these scale-breaking fits was typically 1.2 - 1.6 per degree of freedom. Over the full range of x, the best-fit values for $1/\Lambda_1^2$ and $1/\Lambda_2^2$ were essentially the same for the proton, but were different by about 2 standard deviations for the case of the deuteron. This difference may well have arisen from smearing effects[11,13] or resonance contributions[15] at low W, for $1/\Lambda_1^2$ and $1/\Lambda_2^2$ were equal within one standard deviation when the deuteron data were restricted to $W \geq 2.6$ GeV. When the fitted data were restricted to $x > 0.3$, the best fit values of $1/\Lambda_i^2$ increased by less than one standard deviation. For this region of x, the coefficients for the scale-breaking form $h_i(Q^2) = 1 - 2Q^2/\Lambda_i^2$ are in agreement with the values $1/\Lambda_1^2 = 0.0162 \pm 0.0024$ and $1/\Lambda_2^2 = 0.0134 \pm 0.0013$ obtained earlier[4] for $0.33 \leq x \leq 0.67$ using data from experiments A and C. The results for $1/\Lambda_1^2$ in the propagator scale-breaking form are also in agreement with the results of similar fits to recent data[33] for $2MW_1^p$ in the range $0.4 \leq x \leq 0.9$, where a value of $1/\Lambda_1^2 = 0.0233 \pm 0.0008$ was reported. For $x < 0.3$, both the separated proton and deuteron structure functions were all consistent with scaling in ω, within two standard deviations. A comparison of these fits with the structure function data is presented in Fig. 13, where ratios $F_i(x,Q^2)/f_i(\omega)$ have been plotted versus Q^2 at fixed x. The polynomial functions f_i correspond to the structure function fits of the form $F_i(x,Q^2) = f_i(\omega)(1-2Q^2/\Lambda_i^2)$ to all the data in the kinematic range $W \geq 2$ GeV, $Q^2 \geq 2$ GeV^2, $0.1 \leq x \leq 0.8$, as listed in Table 5. The solid lines represent the best fits to these data of the linear scale breaking form.

The best-fit parameters $1/\Lambda_1^2$ and $1/\Lambda_2^2$ of fits to F_1 and F_2 using the scaling variable $\xi = \omega'$ are presented in Table 6. Systematic uncertainties in these quantities were estimated in the same manner as they were for $\xi = \omega$, and

TABLE 6

Deviations from scaling in ω', from least-square fits of the form $F_i(x,Q^2) = f_i(\omega')h_i(Q^2)$ to the proton data only.

x range	$h_i(Q^2) = 1 - 2Q^2/\Lambda_i^2$		$h_i(Q^2) = (1 + Q^2/\Lambda_i^2)^{-2}$	
	$1/\Lambda_1^2$	$1/\Lambda_2^2$	$1/\Lambda_1^2$	$1/\Lambda_2^2$
$0.1 \leq x \leq 0.8$	0.0044±0.0024	0.0054±0.0012	0.0047±0.0030	0.0059±0.0015
$0.3 \leq x \leq 0.8$	0.0052±0.0025	0.0055±0.0013	0.0059±0.0031	0.0061±0.0017

are included in the errors quoted in Table 6. Except at $x < 0.3$, the two scale-breaking functions provided better fits to the data than the exact scaling form $F_i(x,Q^2) = f_i(\omega')$. The χ^2 for the fits listed in Table 6 ranged from 0.7 to 1.1 per degree of freedom; the two proton structure functions are consistent with scaling in ω' modified by either scale-breaking form. For the full range of x, the best-fit parameters $1/\Lambda_1^2$ and $1/\Lambda_2^2$ are equal for the proton, with errors; νW_2^p is inconsistent with scaling in ω', while $2MW_1^p$ is barely consistent, at the two standard deviation level. For this same range of x, νW_2^d is consistent with scaling in ω', but $2MW_1^d$ is not. For the range $0.3 \leq x \leq 0.8$, the coefficients for the linear scale-breaking form are consistent with the values $1/\Lambda_1^2 = 0.0049 \pm 0.0035$ and $1/\Lambda_2^2 = 0.0020 \pm 0.0018$ reported earlier for $0.33 \leq x \leq 0.67$ using data from experiments A and C.[4] The results for $1/\Lambda_1^2$ in the propagator form are also in agreement with the results of similar fits to the recent data for $2MW_1^p$ in the range $0.4 \leq x \leq 0.9$, where a value of $1/\Lambda_1^2 = 0.0078 \pm 0.0006$ was reported.[33] In the range $0.1 \leq x \leq 0.3$, no violation of scaling in ω' was observed.

For the separated proton structure function data restricted to the kinematic region ($W \geq 2.0$, $Q^2 \geq 2.0$, $x \geq 0.3$), the results of our scaling tests are

unambiguous. Both structure functions are inconsistent with scaling in ω, and νW_2^p is inconsistent with scaling in ω'. The structure function $2MW_1^p$ shows a violation of scaling in ω' that is equal to that exhibited by νW_2^p, but the errors are larger and preclude a completely conclusive result. Over the range of Q^2 ($2.0 \leq Q^2 \leq 16.0$ GeV^2) studied in these tests, we see a 40% violation of scaling in ω and a 15% violation of scaling in ω', for $x \geq 0.3$. For either scaling variable, no evidence is seen for different values of $1/\Lambda_1^2$ and $1/\Lambda_2^2$, even when we restrict $W \geq 2.6$ GeV, and we conclude that they are equal, within the present errors. Theories[35] in which an anomalous magnetic moment of the nucleon constituents is invoked to explain the rise of $R = \sigma(e^+e^- \rightarrow \text{hadrons})/\sigma(e^+e^- \rightarrow \mu^+\mu^-)$ in electron-positron interactions[37] require that $2MW_1$ should fall faster with Q^2 than νW_2. Such theories are apparently ruled out by the present proton data. One can still obtain scaling of both proton structure functions in some phenomenological scaling variable $\tilde{\omega} = \omega + \tilde{M}^2/Q^2$ with $\tilde{M}^2 \approx 1.5$ GeV^2, as has been done in recent studies[33] of $2MW_1^p$. For the range $0.1 \leq x \leq 0.3$, the two proton structure functions are consistent with scaling in both ω and ω'. The lack of any significant Q^2-dependence in this region, when combined with violations of scaling for $x \geq 0.3$, is consistent with field-theoretic models[38] of nucleon structure.

ACKNOWLEDGEMENTS

We thank C. Sinclair and E. Taylor and the rest of the SLAC Spectrometer Facilities Group for their technical support. We are grateful to K. Stone and K. Tsipis for help in running these experiments and E. Miller and R. Verdier for programming assistance. Special thanks are due W. Atwood for use of his computer programs.

REFERENCES

1. A. Bodek et al., Phys. Rev. Letters 30, 1087 (1973).
2. A. Bodek et al., Phys. Letters 51B, 417 (1974).
3. E. M. Riordan et al., Phys. Rev. Letters 33, 561 (1974).
4. E. M. Riordan et al., Phys. Letters 52B, 249 (1974).
5. J. S. Poucher et al., Phys. Rev. Letters 32, 118 (1974); see also Stanford Linear Accelerator Report No. SLAC-PUB-1309.
6. The 6 and 10 degree inelastic e-p and e-d measurements were made by a collaboration of physicists from MIT and SLAC Group A. The members of that collaboration are the authors of Ref. 5. The cross sections used in this work were radiatively corrected according to the MIT method, as discussed in J. S. Poucher, Ph.D. thesis, Massachusetts Institute of Technology, 1971 (unpublished).
7. G. Miller et al., Phys. Rev. D 5, 528 (1972); see also G. Miller, Stanford Linear Accelerator Report No. SLAC-129 (1971).
8. S. D. Drell and J. D. Walecka, Ann. Phys. 28, 18 (1964).
9. L. N. Hand, Phys. Rev. 129, 1834 (1963); see also L. N. Hand, Ph.D. thesis, Stanford University, 1961.
10. P. N. Kirk et al., Phys. Rev. D 8, 63 (1973) and D. H. Coward et al., Phys. Rev. Letters 20, 292 (1968).
11. A. Bodek, Ph.D. thesis, Massachusetts Institute of Technology, available as MIT Report No. LNS-COO-3069-116 (1972).
12. E. M. Riordan, Ph.D. thesis, Massachusetts Institute of Technology, available as MIT Report No. LNS-COO-3069-176 (1973).
13. A. Bodek et al., to be published.

14. Both sets of elastic e-p cross sections had been radiatively corrected according to the method of Y. S. Tsai, Phys. Rev. 122, 1898 (1961).

15. For example, the behavior of R_n at the position of the elastic peak is expected from local duality arguments to be $R_n \rightarrow (4M^2/Q^2)(G_E^2/G_M^2) = 0$ if $G_E^2(Q^2) = 0$. See References 22 and 29. Similar arguments could be made for R_n at values of W close to the resonance region.

16. A. Bodek, Phys. Rev. D 8, 2331 (1973).

17. R. P. Feynman, Proc. 3rd Int. Conf. on High Energy Collisions, Stony Brook, 5-6 Sept 1969 (Gordon & Breach, New York, 1969); see also R. P. Feynman, Photon-Hadron Interactions (W. A. Benjamin, New York, 1972).

18. C. G. Callan and D. J. Gross, Phys. Rev. Letters 22, 156 (1969).

19. K. T. Mahanthappa and Tsu Yao, Phys. Letters 39B, 549 (1972); J. E. Mandula, Phys. Rev. D 8, 328 (1973).

20. H. Georgi and H. D. Politzer, Phys. Rev. D 9, 416 (1974); D. J. Gross and F. Wilczek, Phys. Rev. D 9, 980 (1974); and D. J. Gross, Phys. Rev. Letters 32, 1071 (1974).

21. D. V. Nanopoulos and G. G. Ross, CERN Preprint No. Ref. TH. 2007-CERN (8 April 1975).

22. J. F. Gunion and R. L. Jaffe, Phys. Rev. D 8, 3215 (1973).

23. J. J. Sakurai, Phys. Rev. Letters 22, 981 (1969).

24. J. J. Sakurai, Phys. Rev. Letters 30, 245 (1973).

25. For a review of ρ-electroproduction data, see the talk by K. Berkelman, in Proc. XVI Int. Conf. on High Energy Physics, Batavia, Ill., 6-13 Sept 1972, J. D. Jackson and A. Roberts, eds. (National Accelerator Laboratory, Batavia, Ill., 1973), Vol. 4, p. 41.

26. R. Jaffe, private communication.

27. S. Stein et al., Stanford Linear Accelerator Report No. SLAC-PUB-1528 (1975), submitted to Phys. Rev.

28. J. D. Bjorken, Phys. Rev. 179, 1547 (1969).

29. E. D. Bloom and F. J. Gilman, Phys. Rev. D 4, 2901 (1971).

30. See, for example, R. Jackiw, Phys. Today 25, 23 (Jan 1972).

31. M. Breidenbach and J. Kuti, Phys. Letters 41B, 345 (1972).

32. V. Rittenberg and H. R. Rubinstein, Phys. Letters 35B, 501 (1972).

33. W. B. Atwood, Ph.D. thesis, Stanford University, available as Stanford Linear Accelerator Center Report No. SLAC-185.

34. M. S. Chanowitz and S. D. Drell, Phys. Rev. Letters 30, 807 (1973), and Phys. Rev. D 9, 2078 (1974); M. Pavkovic, Phys. Letters 46B, 435 (1973).

35. G. B. West and P. Zerwas, Phys. Rev. D 10, 2130 (1974).

36. T. D. Lee, Phys. Today 25, 23 (April 1972); also CERN 73-15 (1973).

37. See the rapporteur's talk by B. Richter in Proc. XVII Int. Conf. on High Energy Physics, London, 1-10 Jul 1974, J. R. Smith, ed. (Rutherford Laboratory, Chilton, England, 1974).

38. K. G. Wilson, Phys. Rev. 179, 1499 (1969); G. Parisi, Phys. Letters 43B, 207 (1973); see also Wu-Ki Tung, University of Chicago Preprint No. EFI-75/14 (1975) and No. EFI-75/36 (1975).

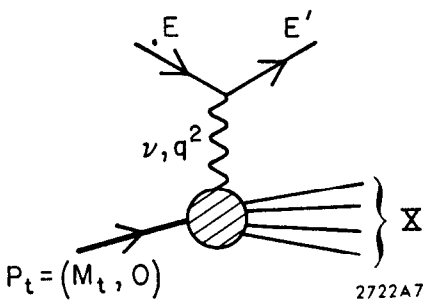

FIG. 1--Feynman diagram for inelastic e-nucleus scattering in the first Born approximation. The mass of the target nucleus is M_t and the final state X is unobserved.

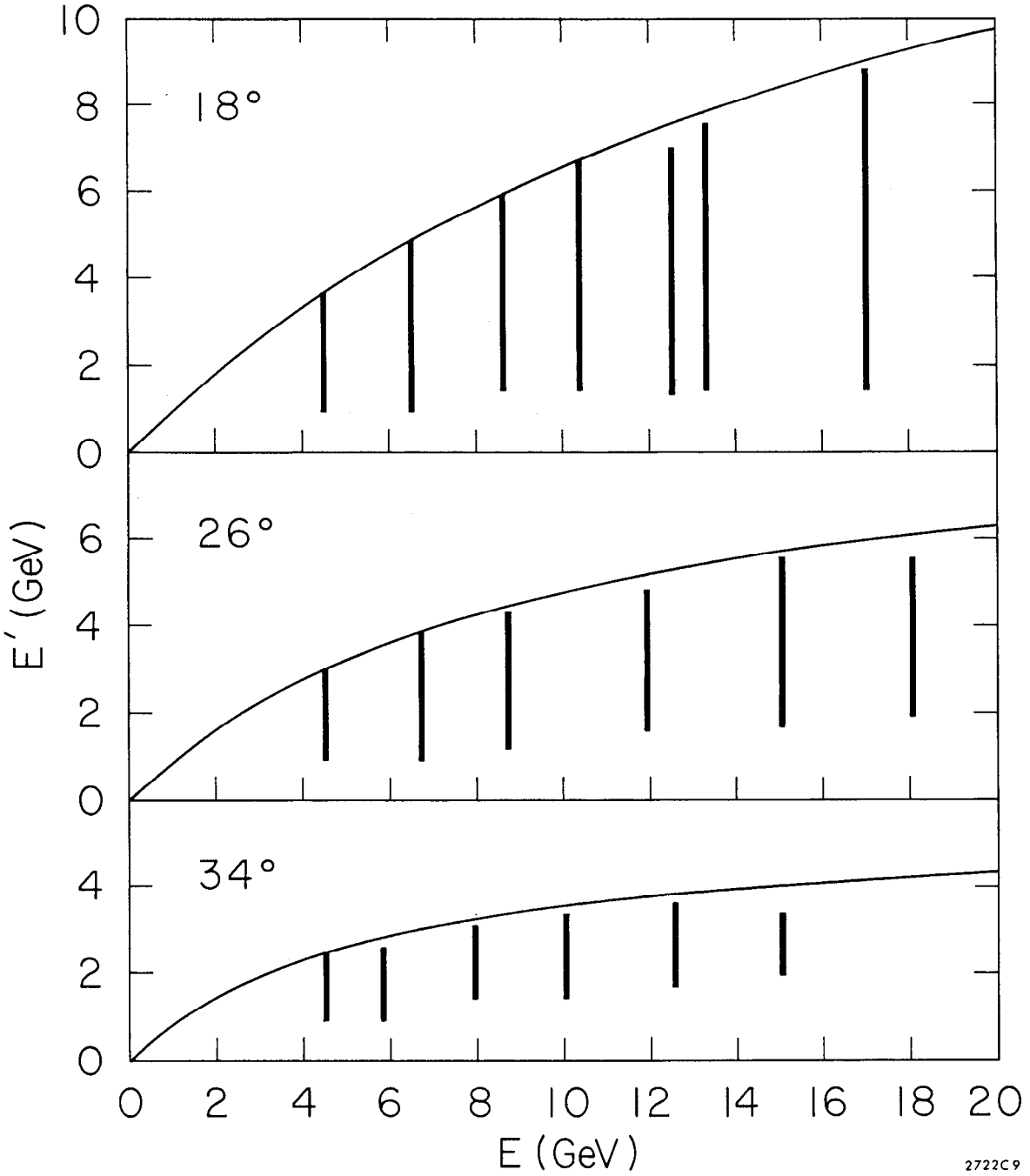

FIG. 2--The incident energies E and the ranges of scattered energy E' for which cross sections were measured at scattering angles of 18, 26, and 34 degrees in experiment A. The totality of data measured at a single scattering angle is frequently referred to as a "triangle".

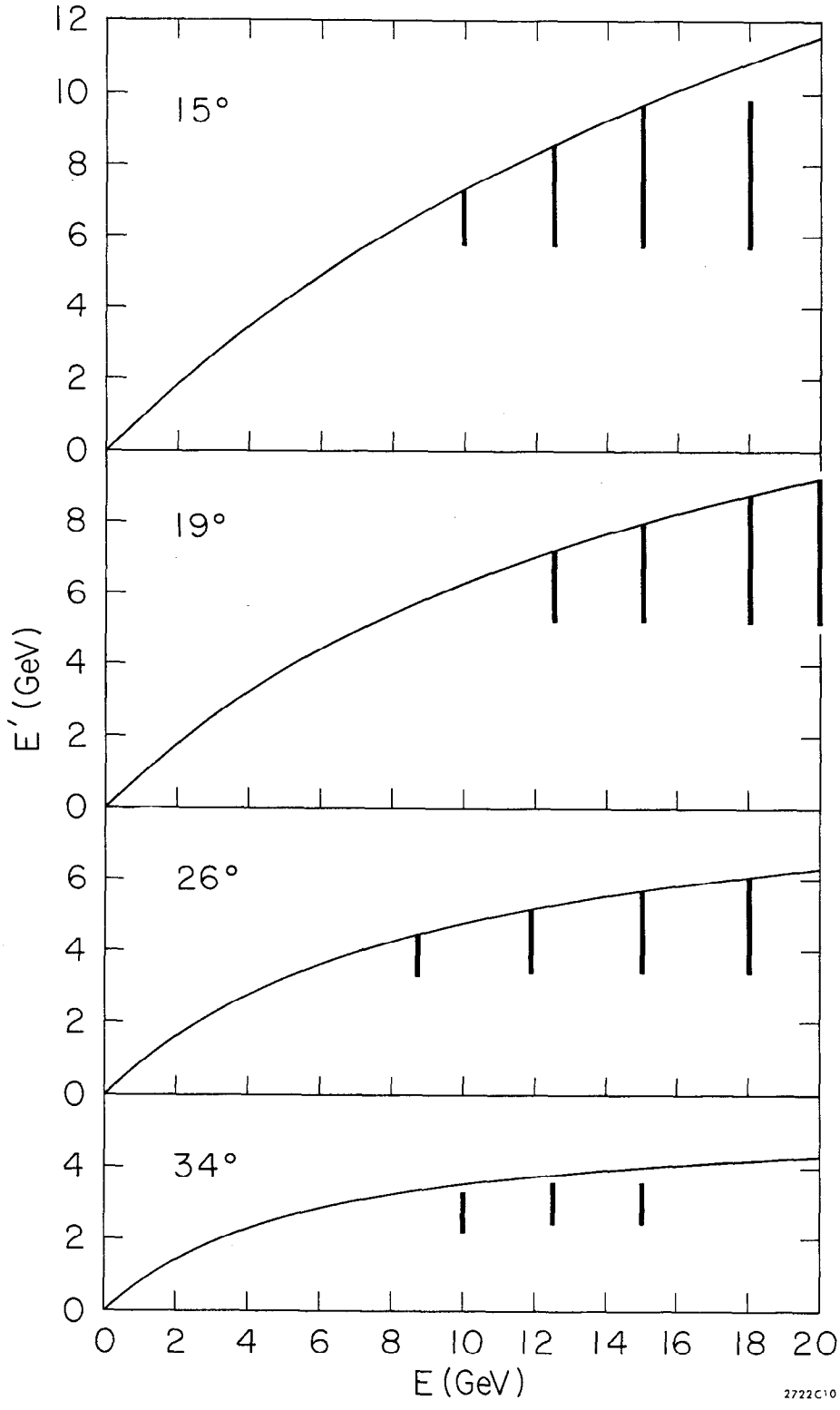

FIG. 3--The incident energies E and ranges of scattered energy E' for which cross sections were measured at scattering angles of 15, 19, 26, and 34 degrees in experiment B.

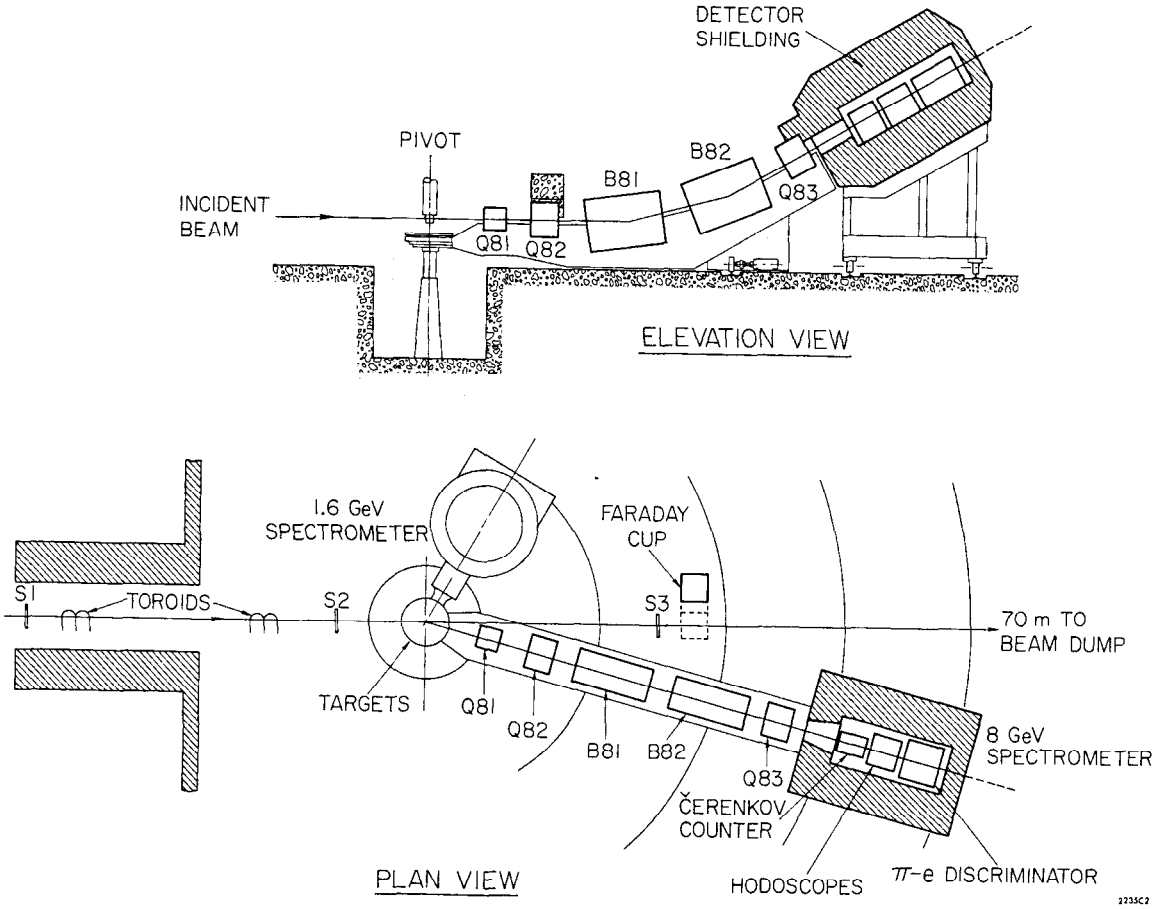

FIG. 4--The experimental setup used to measure inelastic e-p and e-d cross sections in experiments A and B.

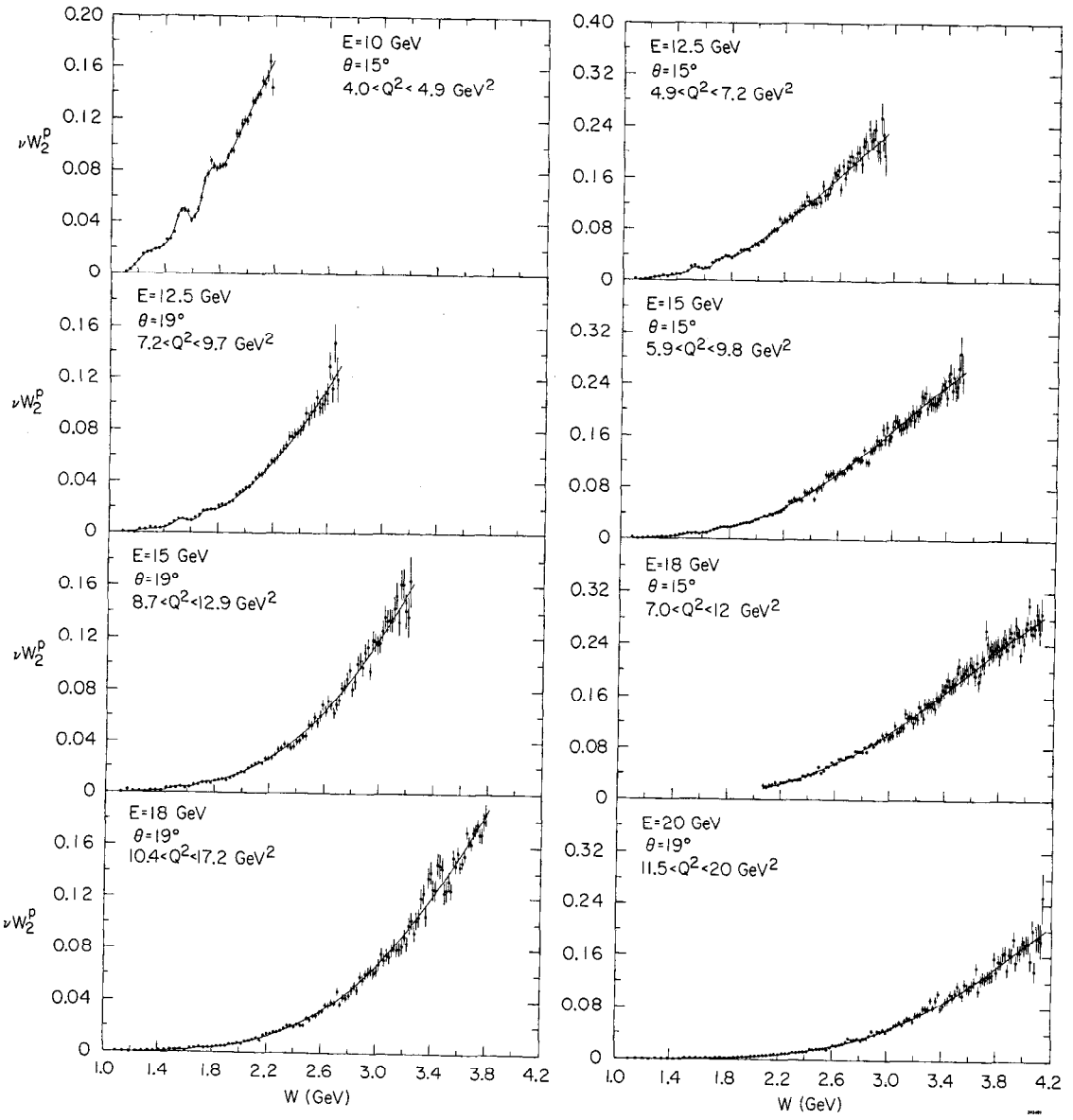

FIG. 5a--The quantity νW_2^p, which was extracted from inelastic e-p cross sections measured at 15° and 19° in experiment B by assuming $R_p = 0.18$. The error bars shown represent only random errors from counting statistics.

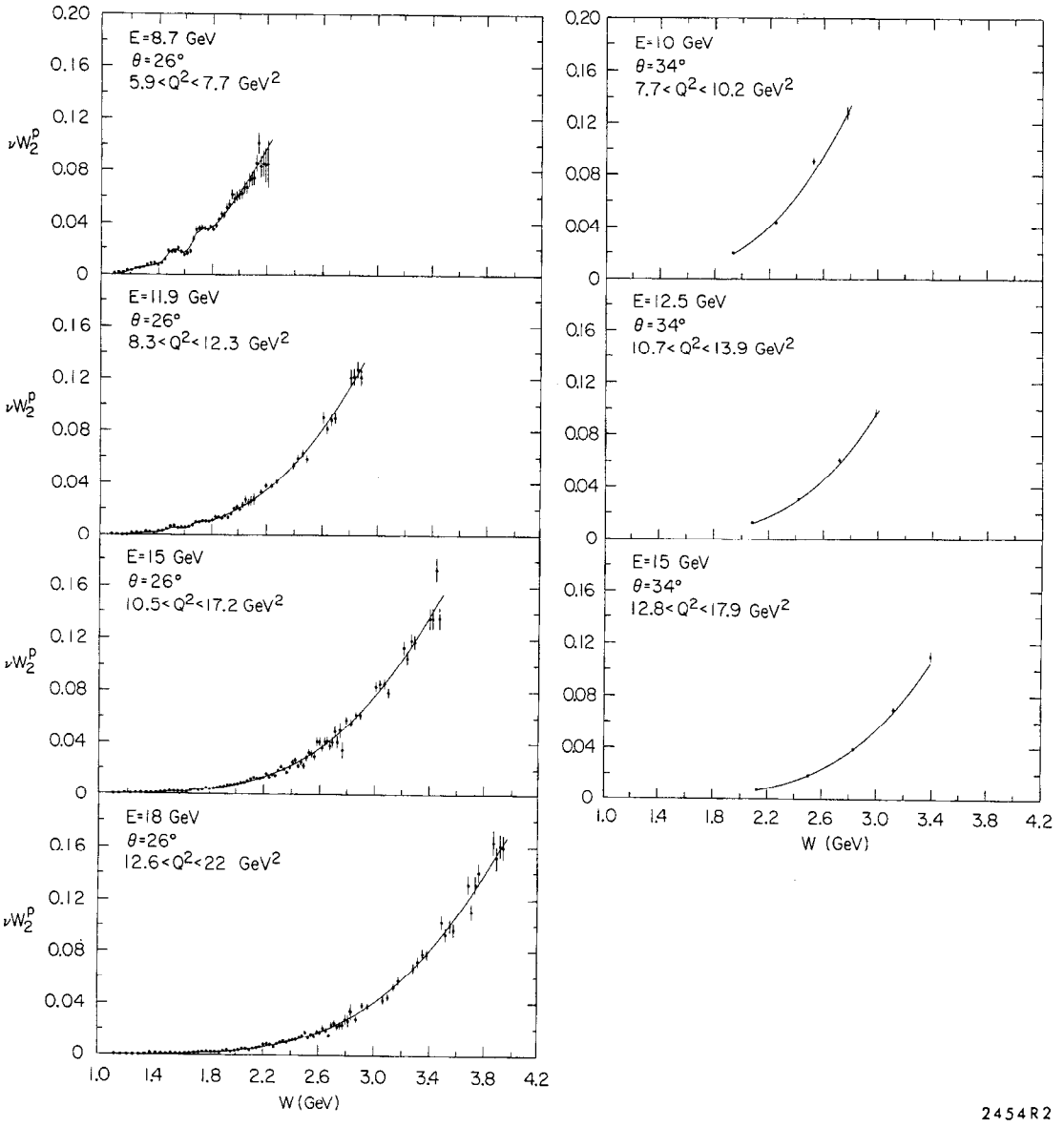

FIG. 5b--The quantity νW_2^p, which was extracted from inelastic e-p cross sections measured at 26° and 34° in experiment B by assuming $R_p = 0.18$. The error bars shown represent only random errors from counting statistics.

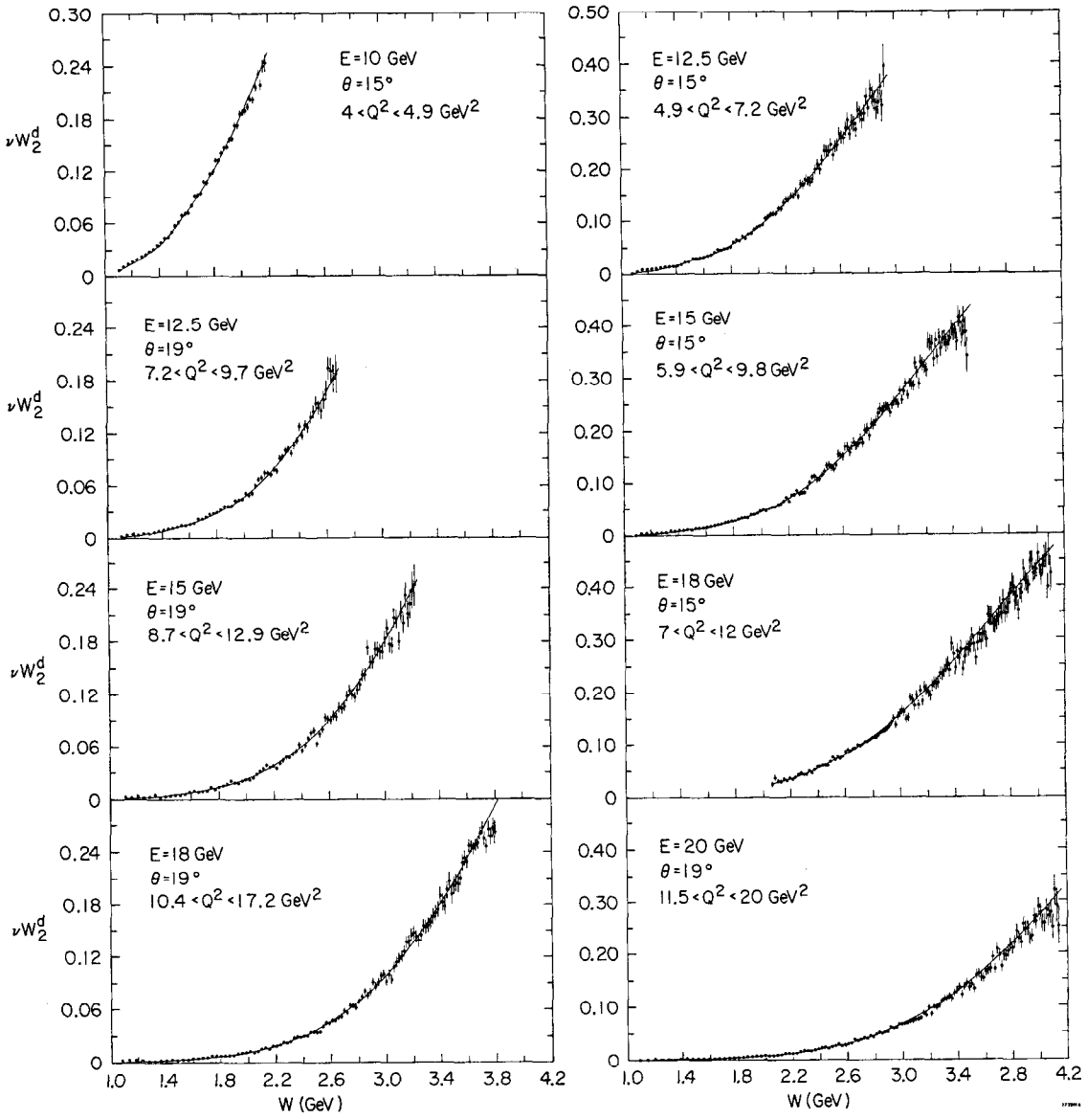

FIG. 6a--The quantity νW_2^d, which was extracted from inelastic e-d cross sections measured at 15° and 19° in experiment B by assuming $R_d = 0.18$. The error bars shown represent only the random errors from counting statistics.

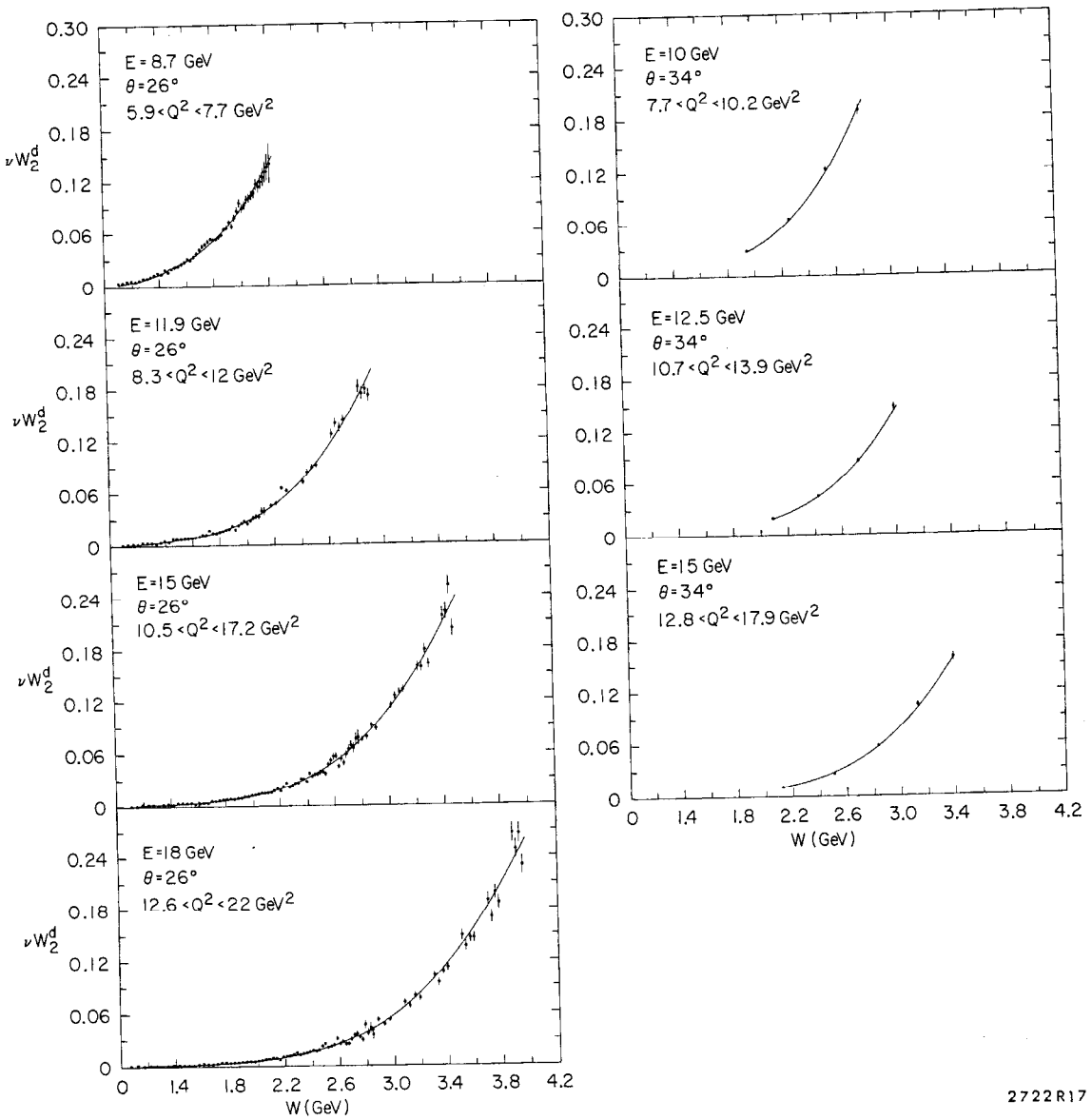

FIG. 6b--The quantity νW_2^d, which was extracted from inelastic e-d cross sections measured at 26° and 34° by assuming $R_d = 0.18$. The error bars shown represent only the random errors from counting statistics.

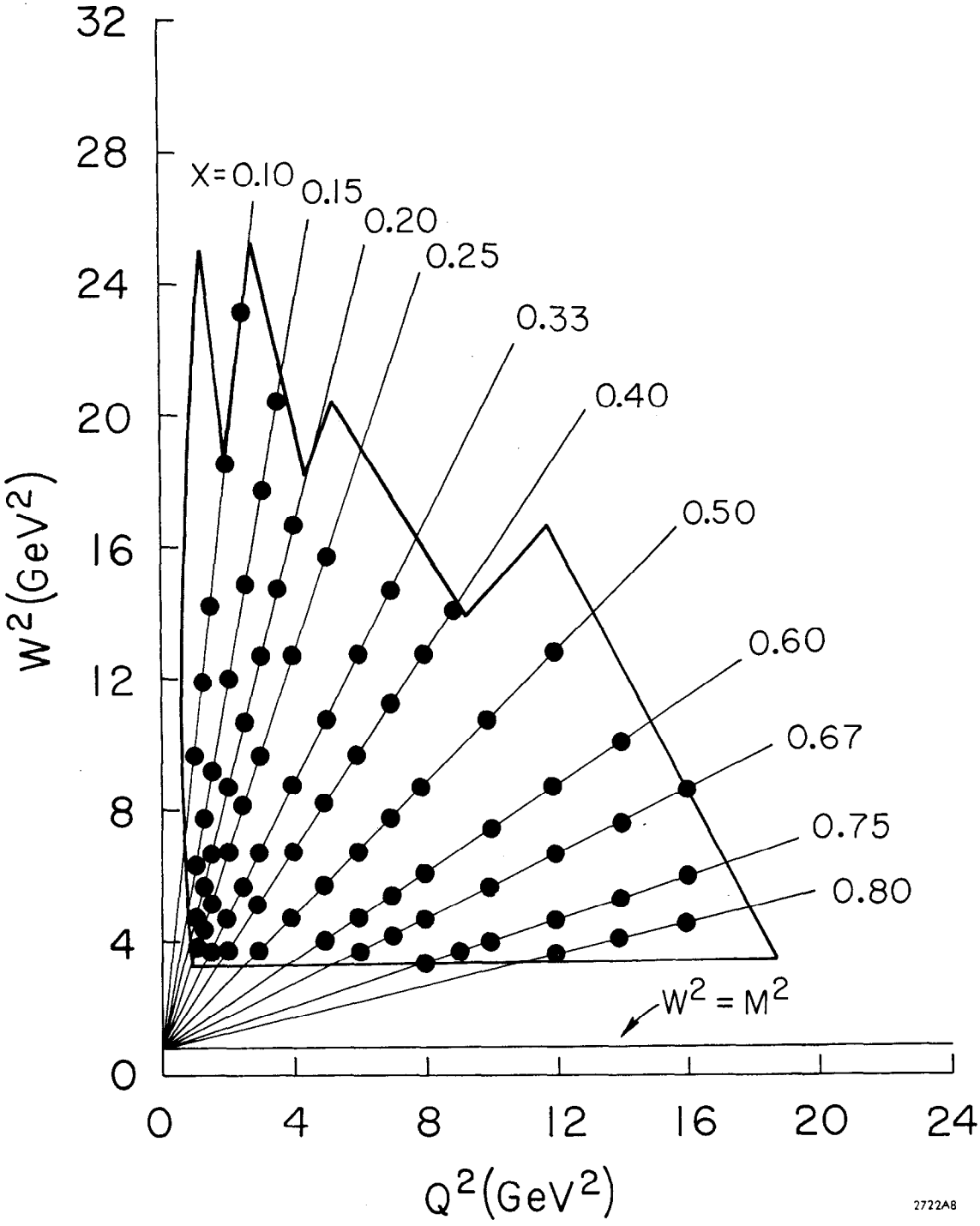

FIG. 7--The kinematic region of Q^2-W^2 space available for separation of R and the structure functions. The heavy solid line delimits the regions where two or more of the measured data triangles overlap. Separations were made at the 75 kinematic points (ν, Q^2) shown.

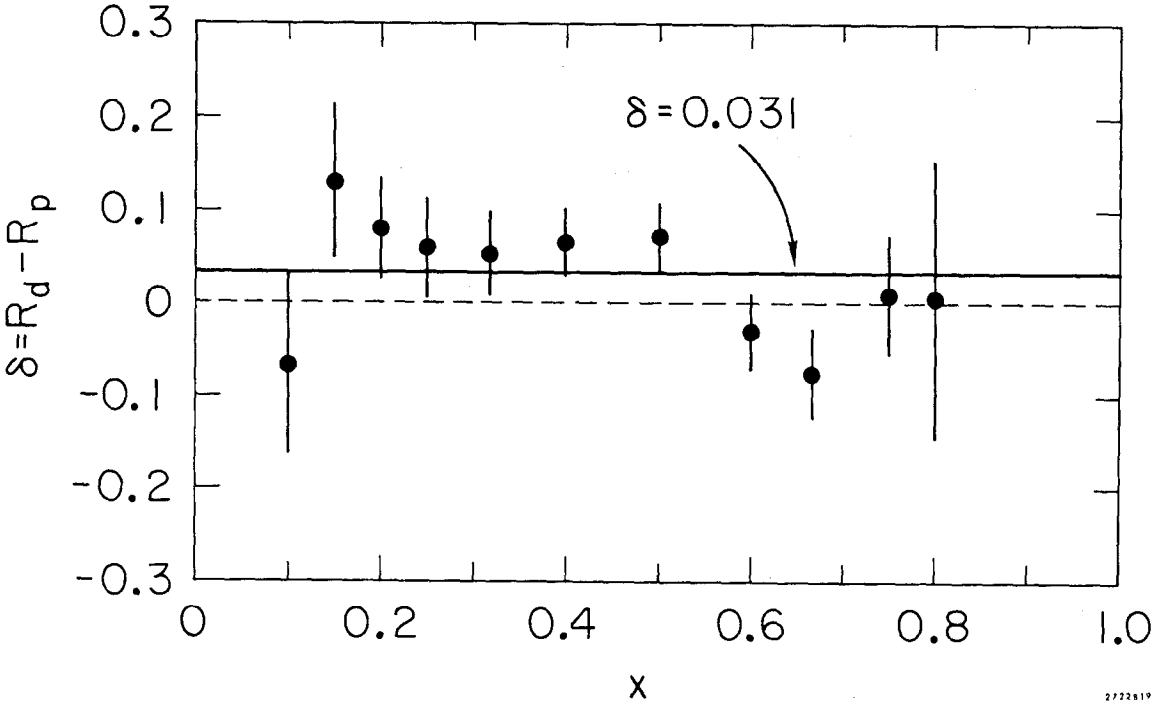

FIG. 8--Average values of the quantity $\delta = R_d - R_p$ for each of the 11 values of x studied. Errors shown are purely random errors.

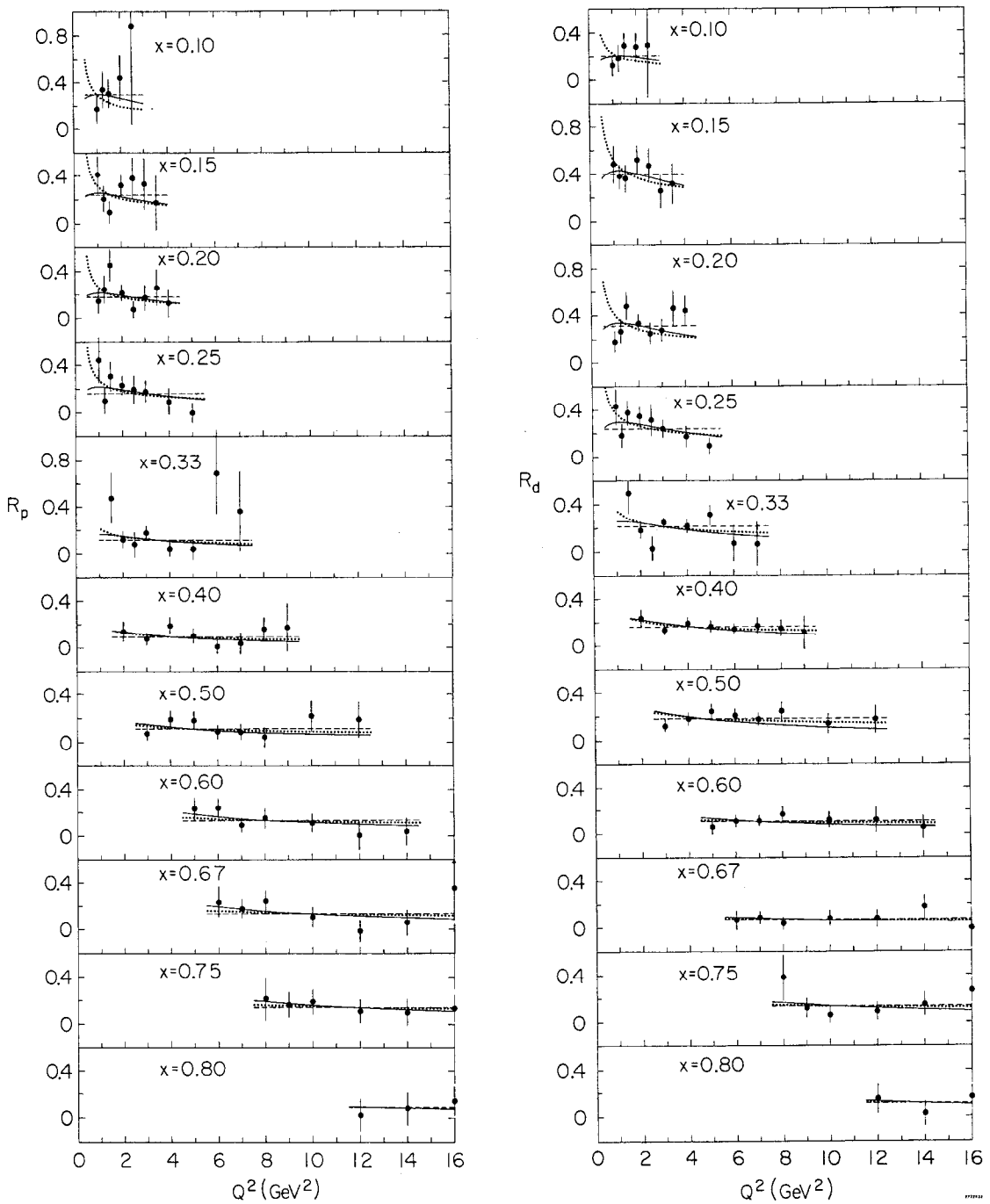

FIG. 9--The quantities R_p and R_d plotted versus Q^2 for the 11 fixed values of x studied. Errors shown in these plots are purely random errors. The dashed lines represent constant fits to R_p and R_d at each value of x. The solid lines and dotted lines represent fixed-x fits of the form $R = c(x)Q^2/(Q^2 + d^2)^2$ and $R = \alpha^2(x)/\ln(Q^2/\beta^2)$ at each value of x.

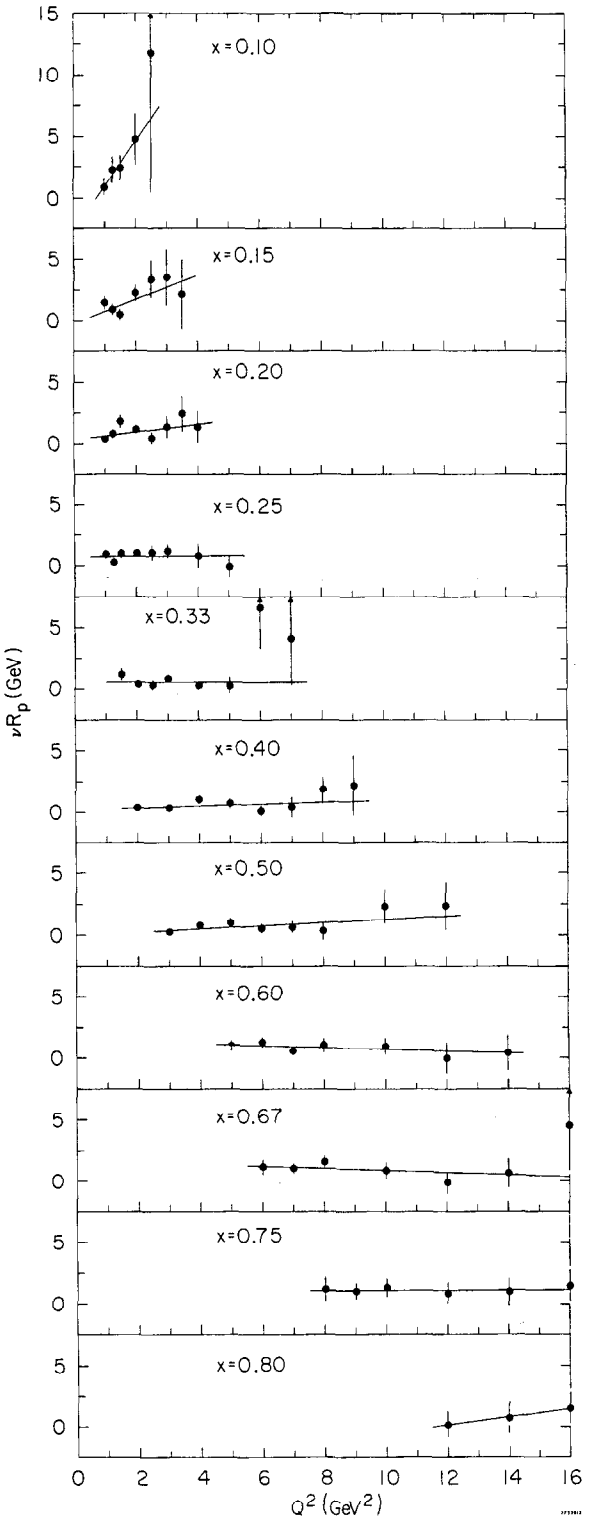

FIG. 10--The quantity νR_p plotted versus Q^2 for the 11 fixed values of x studied. The solid lines represent least-square fits of the form $\nu R_p = a + b\nu = a + \frac{b}{2Mx} Q^2$ to the data at each value of x. The error bars shown represent only the random errors.

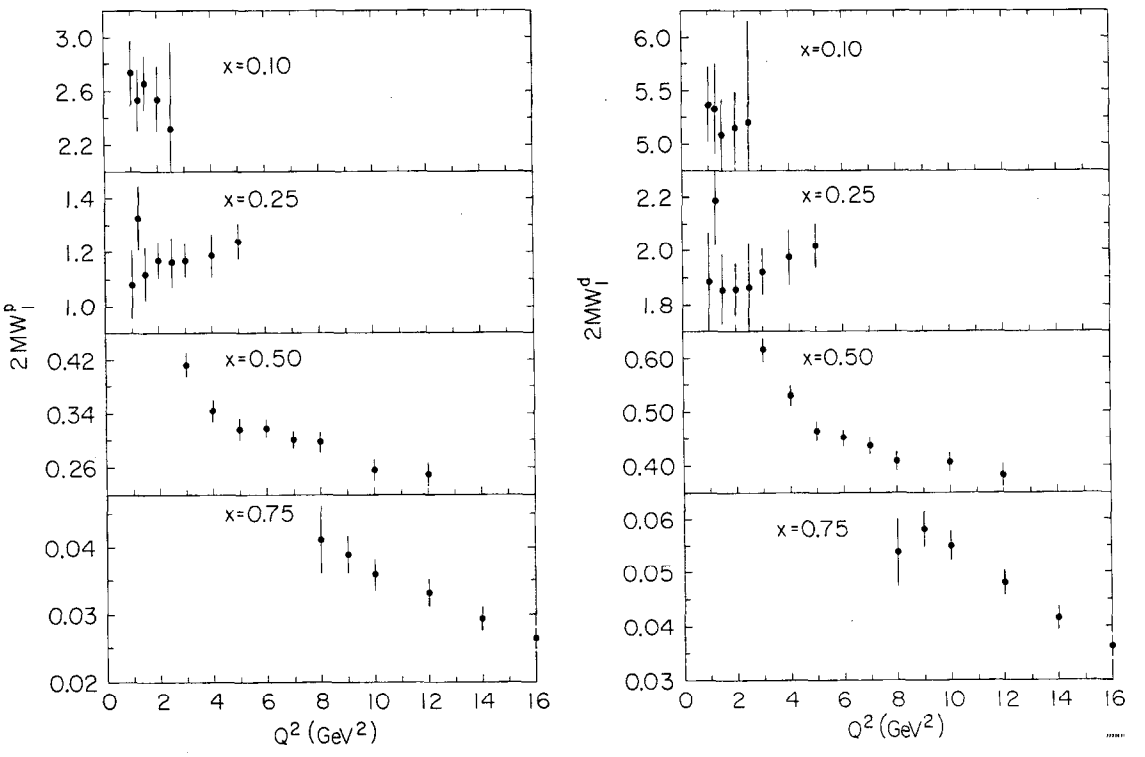

FIG. 11--Separated values of $2MW_1^p$ and $2MW_1^d$ plotted versus Q^2 for selected fixed values of x. The error bars shown represent only the random errors in these quantities.

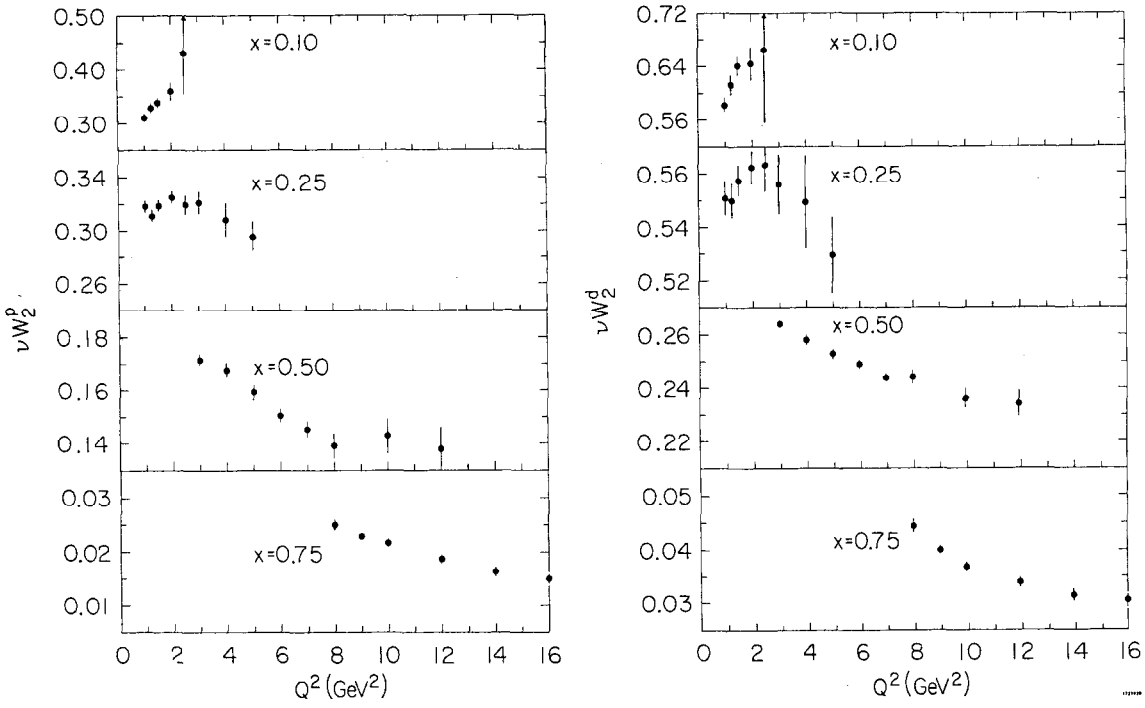

FIG. 12--Separated values of νW_2^p and νW_2^d plotted versus Q^2 for selected fixed values of x. The error bars shown represent only the random errors in these quantities.

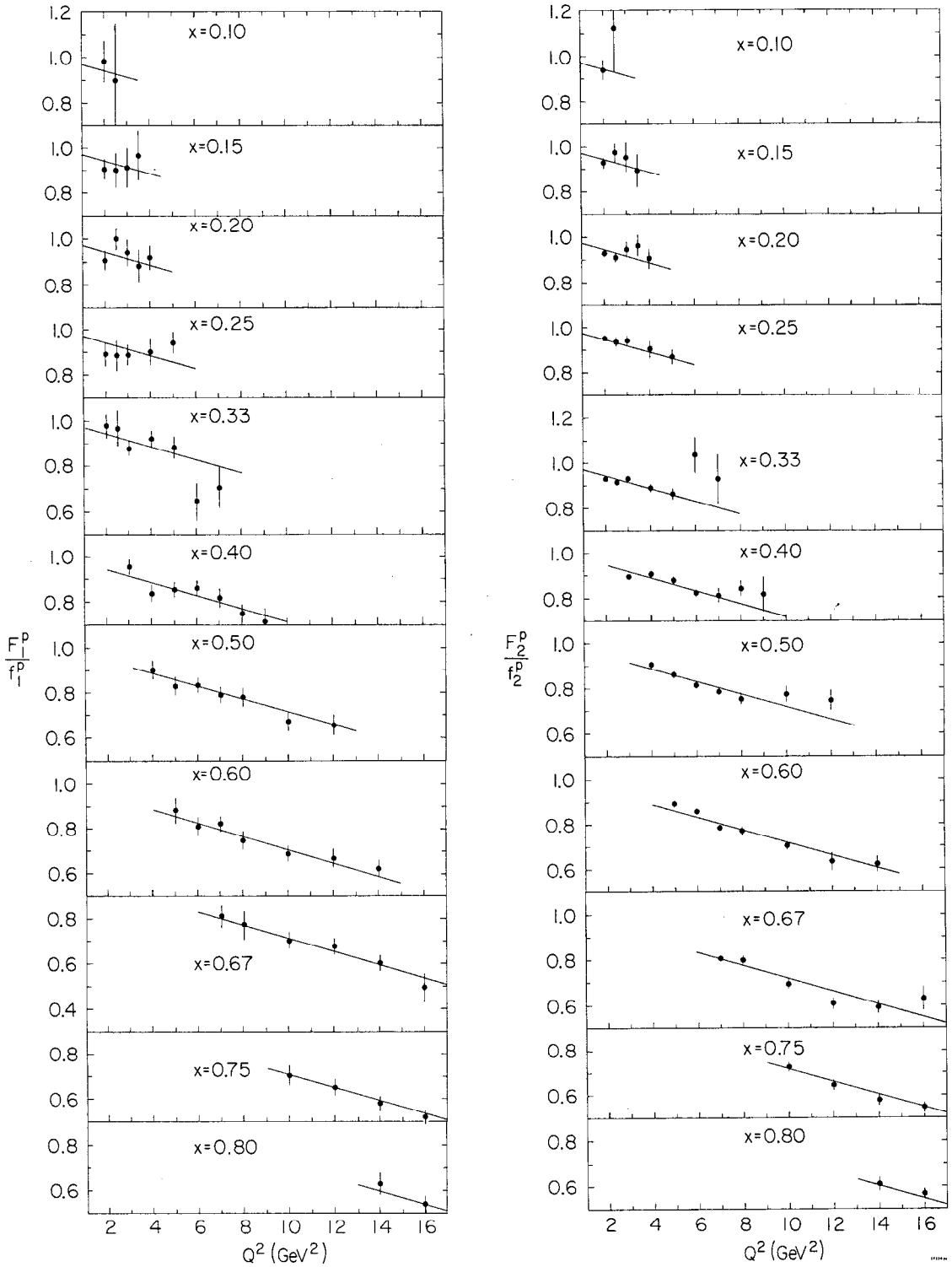

FIG. 13--Ratios of $F_1 = 2MW_1^p$ and $F_2 = \nu W_2^p$ to the polynomials $f_1(x)$ and $f_2(x)$ taken from least-square fits of the form $F_i(x,Q^2) = f_i(x)(1 - 2Q^2/\Lambda_i^2)$ to all the data for $W \geq 2.0$ GeV and $Q^2 \geq 2.0$ GeV^2 in Table 4. The solid lines represent the Q^2-dependent term $(1 - 2Q^2/\Lambda_i^2)$ with $1/\Lambda_1^2$ and $1/\Lambda_2^2$ taken from the case $0.1 \leq x \leq 0.8$ in Table 5. The error bars shown represent only the random errors in the separated quantities F_1 and F_2.